Biophysical Chemistry 293 (2023) 106933

Contents lists available at ScienceDirect

Biophysical Chemistry

journal homepage: www.elsevier.com/locate/biophyschem

A large HIV gp41 construct with trimer-of-hairpins structure exhibits V2E mutation-dominant attenuation of vesicle fusion and helicity very similar to V2E attenuation of HIV fusion and infection and supports: (1) hairpin stabilization of membrane apposition with larger distance for V2E; and (2) V2E dominance by an antiparallel β sheet with interleaved fusion peptide strands from two gp41 trimers

Md Rokonujjaman, Abdulrazak Sahyouni, Robert Wolfe, Lihui Jia, Ujjayini Ghosh, David P. Weliky *

Department of Chemistry, Michigan State University, East Lansing, MI 48824, USA

ARTICLE INFO

Keywords:
HIV
gp41
Fusion peptide
V2E
Dominance
Membrane fusion

ABSTRACT

There is complete attenuation of fusion and infection mediated by HIV gp160 with gp41 subunit with V2E mutation, and also V2E dominance with WT/V2E mixtures. V2E is at the N-terminus of the ~25-residue fusion peptide (Fp) which likely binds the target membrane. In this study, large V2E attenuation and dominance were observed for vesicle fusion induced by FP_HM, a large gp41 ectodomain construct with Fp followed by hyperthermostable hairpin with N- and C-helices, and membrane-proximal external region (Mper). FP_HM is a trimer-of-hairpins, the final gp41 structure during fusion. Vesicle fusion and helicity were measured for FP_HM using trimers with different fractions (f's) of WT and V2E proteins. Reductions in FP_HM fusion and helicity vs. f_{V2E} were quantitatively-similar to those for gp160-mediated fusion and infection. Global fitting of all V2E data supports 6 WT gp41 (2 trimers) required for fusion. These data are understood by a model in which the ~25 kcal/mol free energy for initial membrane apposition is compensated by the thermostable hairpin between the Fp in target membrane and Mper/transmembrane domain in virus membrane. The data support a structural model for V2E dominance with a membrane-bound Fp with antiparallel β sheet and interleaved strands from the two trimers. Relative to $f_{V2E} = 0$, a longer Fp sheet is stabilized with small f_{V2E} because of salt-bridge and/or hydrogen bonds between E2 on one strand and C-terminal Fp residues on adjacent strands, like R22. A longer Fp sheet results in shorter N- and C-helices, and larger separation during membrane apposition which hinders fusion.

1. Introduction

Fusion (joining) of two membranes is important in both physiologically-beneficial and pathogenic processes [1–4]. Fusion is thought to follow a stepwise mechanism with distinct membrane structural intermediates. One common mechanistic model is: (1) close

Abbreviations: A, percent activity; CD, circular dichroism; DPC, dodecylphosphocholine detergent; Ed, ectodomain; ext, extent; F, fluorescence; FHa2, Ha2 ectodomain; Fp, fusion peptide; FP_HM, gp41 ectodomain construct with fusion peptide followed by thermostable hairpin and Mper; gp41/120/160, glycoprotein with 41/120/160 kDa mass; Ha2, influenza hemagglutinin protein subunit 2; HIV, human immunodeficiency virus; IPTG, isopropyl β-D-1-thiogalactopyranoside; LB, Luria-Bertani; M, percent vesicle fusion; Mper, membrane-proximal external region; POPC, 1-palmitoyl-2-oleoyl-phosphatidylcholine; POPG, 1-palmitoyl-2-oleoyl-phosphatidylglycerol; R, fluorophore/quencher distance; R_{For}, Forster distance; SDS, sodium dodecylsulfate detergent; SEC, size-exclusion chromatography; T, number of gp160 trimers required for efficient HIV fusion and infection; Tris/SDS, 10 mM Tris buffer at pH 7.4 with 0.2% SDS; Tmd, transmembrane domain; WT, Wild-type; θ_{222}, circular dichroism mean residue molar ellipticity at 222 nm.

* Corresponding author.
E-mail address: weliky@chemistry.msu.edu (D.P. Weliky).

https://doi.org/10.1016/j.bpc.2022.106933
Received 29 September 2022; Received in revised form 13 November 2022; Accepted 14 November 2022
Available online 24 November 2022

(nm) apposition of the two membranes; (2) formation of a bilayer "stalk" that connects the two membranes and is contiguous with their outer leaflets; (3) topological transformation of the stalk to a planar "hemifusion" bilayer diaphragm that is contiguous with the inner leaflets of the two membranes; and (4) formation and expansion of pores in the hemifusion diaphragm that result in a single bilayer that encompasses the two bodies [3–5]. Steps 2 and 3 are experimentally detected by lipid mixing between the two membranes and step 4 is detected by contents mixing between the two bodies. A variety of computational approaches have been applied to estimate energy barriers for the different steps with typical values of 25 kcal/mol for step 1 and 10 kcal/mol per step for 2, 3, and 4 [4].

The present study focuses on fusion relevant to the membrane-enveloped human immunodeficiency virus (HIV) which is the pathogen for AIDS, a global disease. There is currently no cure or vaccine for AIDS, but there are therapeutics and prophylactics that control and prevent HIV infection and are typically taken daily. Fusion between the membranes of HIV and a target cell is an early and required step in infection [3,4]. There is consequent deposition of viral genetic material in the cytoplasm which is necessary for viral replication within the cell. Fusion between HIV and target cells is mediated by the viral envelope glycoprotein 160 kDa (gp160) which had been proteolytically-cleaved into N-terminal gp120 and C-terminal gp41 subunits, that are respectively ~500 and 350 residues. Gp41 has a ~ 180-residue N-terminal ectodomain (Ed) outside the viral membrane which assembles as a trimer and non-covalently associates with three gp120 subunits to form a spike in the viral envelope [6,7]. There is a single transmembrane domain (Tmd) C-terminal of the gp41 Ed followed by a ~ 150-residue endodomain inside the virus. The first step in infection is gp120 binding to the CD4 receptor and then the CXCR4 or CCR5 chemokine receptor of immune system cells like T-cells and macrophages. This is followed by separation of gp120 from the gp41 Ed, and then a large structural change of much of the Ed into a hyperthermostable trimer-of-hairpins structure [8–10]. The ~60-residue "N-helices" of three gp41 molecules form a parallel coiled-coil within this structure and are followed by 180° turns so that the three ~60-residue "C-helices" are antiparallel and in van der Waals contact with the external grooves of the N-helix core, i.e. each gp41 molecule is a helical hairpin. There are ~25 gp41 residues N-terminal of the N-helix that are denoted the "fusion peptide" (Fp), Fig. 1 [11]. The Fp has extended irregular structure in the initial gp41/gp120 complex, and is the epitope of some broadly-neutralizing antibodies [6,12–14]. Some Fp residues are thought to bind target membrane early in the fusion process. The Fp alone or with C-terminal hairpin often adopts intermolecular antiparallel β sheet structure in membrane, and can adopt β sheet or helical monomer structure in detergent-rich media [15–25]. There are ~10 residues between the C-helix and Tmd that are part of the "membrane-proximal external region" (Mper) some of which may also bind the viral membrane with predominantly helical structure [26–32]. In some studies, the Mper includes residues that are part of the C-helix in Fig. 1. These residues may bind the viral membrane in the initial gp41 Ed complex with gp120. The Mper also includes linear epitopes of broadly-neutralizing antibodies which also bind the final trimer-of-hairpins structure of gp41 [27,33].

To our knowledge, there aren't yet clear experimental data that elucidate the relative timings of changes in membrane and gp41 Ed structure during fusion. Models of the mechanism of gp41-induced fusion are instead based on data that include the initial and final structures of the gp41 Ed, fusion inhibitors, and computation. The most common type of model posits that some of the thermodynamic energy released as the gp41 Ed changes from the initial complex with gp120 to the final hairpin is converted into activation energy between membrane intermediates [2,34,35]. These models often hypothesize well-defined structural intermediates of the gp41 Ed that catalyze formation of specific membrane intermediates, e.g. separated N- and C-helices that bind to the initial apposed membranes or to the stalk [36–41]. For this overall group of models, the final Ed hairpin is a "post-fusion" state, i.e. most or all of the membrane changes during fusion happen prior to final hairpin formation. A separate type of model posits that the final gp41 hairpin forms prior to membrane fusion and is the fusion-catalytic structure. Some data supporting this model type are: (1) rapid and extensive vesicle fusion induced by large gp41 constructs with hairpin structure; and (2) vesicle, cell-cell, and computational fusion induced by the related influenza virus hemagglutinin subunit 2 (Ha2) protein in the final trimer-of-hairpins state [23,25,33,42–47]. For most models, fusion barriers are also reduced by target membrane-binding by the Fp, and by virus membrane-binding by the Mper (Fig. 1) [32,48–53].

Similar to enzyme mechanisms, a proposed mechanism of gp160-mediated fusion is also supported if the mechanism provides sensible explanations of the effects of gp160 mutations on fusion, with particular emphasis on mutations that greatly impair fusion but don't affect initial assembly of gp160 spikes in the HIV membrane. V2E is this type of point mutation and is located at the N-terminus of the Fp of the gp41 subunit of gp160 (Fig. 1). V2E eliminates fusion between cells expressing gp160 and cells expressing CD4 and chemokine receptors, and also eliminate HIV infection of cells [54]. To our knowledge, V2E is the only gp41 mutation that exhibits dominance in mixed trimers of wild-type (WT) and V2E gp160, with $f_{V2E} \equiv$ fraction V2E and $f_{V2E} = 1 - f_{WT}$. As one example, relative to $f_{V2E} = 0$, $f_{V2E} = 0.09$ results in only 40% cell-cell fusion and HIV infection. The dependences of the reductions in fusion and infection on f_{V2E} have been analyzed with mathematical models to determine a number of WT trimers (T) required for efficient fusion and infection. Different research groups have done the analysis using the same or similar data, and the derived values of T depend strongly on the assumptions of the model used in the analysis, with variation in T between 1 and 19 trimers among the different analyses [55]. The large range for T makes it more difficult to distinguish between different possible mechanisms of gp160-mediated fusion. As one consideration, the typical virion has only ~15 trimers, so the fusion rate and viral infectivity might be predicted to be inversely-correlated with T [56]. As an example, if $T = 1$, each trimer could independently catalyze fusion,

Fig. 1. Amino acid sequence of the Wild-type FP_HM construct with 50 residues per line. The sequence is from the HXB2 laboratory strain of HIV. The DNA sequence is displayed in Fig. S1. The construct contains HIV gp41 residues 1–70 and 117–172 separated by SG_2RG_2 non-native linker, with additional G_6LEH_6 non-native C-terminal tag for affinity purification. Residues 1–70 with gp41 numbering correspond to 512–581 with gp160 numbering, and 117–172 correspond to 628–683 numbering. Much of FP_HM adopts thermostable hairpin structure like the final state of the soluble ectodomain of gp41 without gp120 (Fig. 8). For gp41, the hairpin has a N-helix (residues 24–84/535–595) and C-helix (residues 104–164/615–675) that are in close contact and antiparallel with an intervening turn (Fig. 8). There is colour coding of the FP_HM segments that are part of N- and C-helices, and different colors for regions that contain the N-terminal fusion peptide and membrane-proximal external region that respectively bind target cell and viral membrane.

whereas if $T = 15$, fusion requires concerted action of all trimers of the virion. On the other hand, fusion could be faster when T is larger because of summation of multiple gp160-associated reductions in energy barriers between fusion intermediates. T may also be the approximate number of trimers in the local region of the viral membrane undergoing fusion. This hypothesis is correlated with electron micrographs of virions that are bound to target cells prior to fusion. The inter-membrane electron density in the micrographs has been interpreted to be due to a cluster of gp160 trimer ectodomains bound to cellular receptors [57].

It isn't clear why the V2E N-terminal point mutation of gp41 greatly attenuates gp160-mediated fusion and HIV infection, in part because there aren't clear data about the differences in V2E vs. WT structures. Structure-function studies to-date have focused on ~25-residue peptides with the Fp sequence. Peptide-induced vesicle fusion was attenuated for V2E vs. WT, but to our knowledge, V2E dominance has not been observed for WT + V2E peptide mixtures [58–60]. Comparative structural studies have been done for the WT and V2E peptides in detergent and in membrane. For either peptide, there are populations of molecules with either predominant helical or β sheet structures. The different studies present conflicting data about the helical:β sheet ratio for V2E vs. WT, and include reports of larger, smaller, or no change in ratio [60–64]. There are similarly conflicting data about whether relative to WT, V2E has shallower or deeper location in the micelle or membrane.

The present study addresses unresolved questions about the mechanism of HIV fusion and its V2E-dominant attenuation, and includes a new model for V2E attenuation based on data from the present and earlier studies. The study focuses on the large Ed "FP_HM" construct which includes the Fp followed by the hyperthermostable ($T_m > 100$ °C) hairpin, i.e. the final gp41 structural state (Fig. 1) [25,33,44,65]. Earlier studies showed that vesicle fusion induced by FP_HM has significant similarities with gp160-induced cell/cell fusion, and under some conditions, FP_HM induces vesicle fusion with protein:lipid mole ratio ≈ 1:5000 similar to the gp160:lipid ratio in virions [33]. The present study investigates whether fusion is highly-attenuated for V2E FP_HM and also whether V2E is dominant in mixed WT/V2E FP_HM trimers. Observation of these effects would support an important catalytic role for the final gp41 hairpin state in HIV fusion and also provide other information about the fusion mechanism.

2. Materials and methods

2.1. Materials

Commercial sources included: DNA, GenScript (Piscataway, NJ); *Escherichia coli* (*E. coli*) Novagen (Gibbstown, NJ); Luria-Bertani (LB) medium, Dot Scientific (Burton, MI); isopropyl β-D-thiogalactopyranoside (IPTG), Goldbio (St. Louis, MO); and Co^{2+} affinity resin, Thermo Scientific (Waltham, MA). Avanti Polar Lipids (Alabaster, AL) was the source for lipids that included 1-palmitoyl-2-oleoyl-*sn*-glycero-3-phosphocholine (POPC), 1-palmitoyl-2-oleoyl-*sn*-glycero-3- [phospho-*rac*-(1-glycerol)] (sodium salt) (POPG), *N*-(7-nitro-2,1,3-benzoxadiazol-4-yl) (ammonium salt) Dipalmitoylphosphatidylethanolamine} (*N*-NBD-DPPE) and *N*-(lissamine Rhodamine B sulfonyl) (ammonium salt) dipalmitoylphosphatidylethanolamine} (*N*-Rh-DPPE). Other materials were typically purchased from Sigma-Aldrich (St. Louis, MO).

2.2. FP_HM constructs, expression, and purification

FP_HM proteins were produced using *E. coli* BL21(DE3) cells that were typically incubated at 37 °C in LB medium with kanamycin (50 mg/mL) and shaking at 150 rpm. Fig. S1 displays the DNA sequence that coded for the Wild-type (WT) FP_HM sequence and non-native C-terminal G_6LEH_6. The WT sequence with G_6 was subcloned into a pET-24a (+) plasmid with Lac operon and kanamycin antibiotic resistance and the plasmid with insert was transformed into *E. coli* cells. After culture growth in LB medium, the plasmid was extracted from a culture aliquot followed by PCR with DNA primers (Fig. S2) to produce a plasmid with V2E + G6 DNA that was subsequently transformed into *E. coli* cells. The WT and V2E inserts were confirmed by DNA sequencing of their respective extracted plasmids. WT and V2E culture stocks were separately prepared by streaking cells onto an agar plate, overnight growth, single colony selection, overnight growth in 50 mL LB medium, and mixing 1 mL culture aliquot and 0.5 mL 50% (*v*/v) glycerol with storage at −80 °C.

FP_HM production began with addition of 75 μL bacterial glycerol stock to 50 mL LB medium, ~7 h culture growth, transfer to 1 L fresh LB medium, and ~ 3 h growth. The growth times resulted in final OD_{600}'s of ~0.8. Expression was induced by addition of 2 mmole IPTG followed by incubation at 37 °C for 6 h. The cell pellet was harvested by centrifugation at 9000 *g* for 15 min and stored at −20 °C. For subsequent steps, the PBS pH was 7.4, tip sonication was done with a surrounding ice bath, and centrifugation was done with 48,000 *g* for 30–45 min at 4 °C. FP_HM has low solubility in PBS without additives and was separated from PBS-soluble molecules by 3× repetition of sonication of 5 g cell pellet in 30 mL PBS followed by centrifugation and harvesting the new pellet. The final pellet with FP_HM was then solubilized by sonication in PBS with 8 M urea followed by centrifugation and collection of the supernatant. Some dissolved molecules including FP_HM were then precipitated by increasing [NaCl] to ~300 mM. Subsequent steps were: (1) centrifugation, harvesting, and then vortexing the pellet in distilled water; (2) centrifugation, harvesting, and then pellet dissolution in 20 mL PBS with 6 M GuHCl; (3) centrifugation and collection of the supernatant; and (4) Co^{2+}-affinity chromatography. The chromatography was done in a fritted column with liquid removal by gravity filtration, and all solutions contained PBS with 6 M GuHCl. There was: (1) filtration of 5 mL of resin suspension; (2) resin washing with 10 mL of 10 mM imidazole; (3) addition of the FP_HM-containing supernatant followed by agitation overnight at 4 °C; and (4) sequential washing/elution in 15 mL without imidazole, 10 mL of 10 mM imidazole, 5 mL of 300 mM imidazole, and 10 mL of 600 mM imidazole. The elutions with 300 and 600 mM imidazole were combined and dialyzed overnight against distilled water with consequent precipitation, and the suspension was centrifuged, followed by harvesting and lyophilization of the pellet, and storage at −20 °C.

2.3. Preparation of FP_HM samples including WT/V2E mixtures

Lyophilized FP_HM (either WT or V2E) was typically dissolved in 10 mM Tris buffer at pH 8.0 with 0.17% n-decyl-β-D-maltoside, 2 mM EDTA, and 1 M *L*-arginine. This solution was agitated overnight at 4 °C and then dialyzed against 10 mM Tris buffer at pH 7.4 with 0.2% SDS (Tris/SDS) which is a solution in which FP_HM is predominantly trimeric [25]. The dialysis was for four days with one buffer change. [FP_HM] was then measured using A_{280} and sometimes adjusted with dilution or concentration. Preparation of WT/V2E mixed trimers began with separate solutions of WT and V2E in 200 mM Tris buffer at pH 6.8 with 8% SDS and 400 mM dithiothreitol, which is the solution used for SDS-PAGE in which FP_HM is predominantly monomeric. Mixed trimers with a specific f_{V2E} were formed by combining the appropriate volumes of WT and V2E solutions, followed by dialysis against Tris/SDS.

2.4. Circular dichroism spectroscopy, Size-exclusion chromatography, and Vesicle fusion

Circular dichroism (CD) spectra of FP_HM in Tris/SDS were obtained with a J-810 spectrometer (Jasco; Easton, MD) with sample temperature controlled by a water bath. The quartz cuvette pathlength was 1 mm, and ultraviolet wavelength was scanned in 0.5 nm steps between 190 and 250 nm. Size-exclusion chromatography (SEC) was done using a DuoFlow Pathfinder 20 instrument (Bio-Rad; Hercules, CA) and HiLoad 16/600 Superdex 75 pg column (Cytiva; Marlborough, MA). FP_HM in Tris/SDS (1 mg/mL) was centrifuged at 9000 *g* for 30 min and

chromatography was done with 100 μL injection of the supernatant, Tris/SDS running buffer with flow rate of 1 mL/min, and A_{280} detection.

Preparation of "unlabeled" POPC:POPG (4:1) unilamellar vesicles for vesicle fusion included freeze-thaw cycles (~10×) followed by extrusion (~10×) through a filter with 100 nm diameter pores. A separate set of "labeled" vesicles was similarly prepared and contained additional *N*-NBD-DPPE fluorescent lipid and *N*-Rh-DPPE quenching lipid, with ~0.02 mol fraction for each labeled lipid. The POPC:POPG (4:1) composition was chosen because: (1) these are common lipids used for earlier studies of viral fusion protein constructs; (2) phosphatidylcholine is a common lipid in membranes of host cells of HIV; and (3) the negatively-charged lipid fraction of host cell membranes is represented by the POPG which is negatively-charged over the pH 3.3–7.4 range of the present study [44,66–69]. The target cell outer membrane normally has little anionic lipid, but there is evidence for scramblase-mediated transport of anionic phosphatidylserine lipid from the inner to outer leaflet prior to gp160-mediated fusion [70]. A vesicle solution was prepared with labeled:unlabeled ratio = 1:9, [total lipid] ≈ 150 μM, and typical 25 mM citrate buffer at pH 5.3. The solution was placed in the fluorimeter, warmed to 37 °C, and fluorescence (F) measured at 530 nm using excitation at 467 nm. Initial fluorescence is denoted F_0. An aliquot of stock with [FP_HM] ≈ 150 μM in Tris/SDS was added to the vesicle solution at time $t = 0$, followed by measurement of F(t) to t ≈ 600 s in 1 s increments, with larger uncertainties for $t < 5$ s. Because the ratio of labeled:unlabeled vesicles = 1:9, a labeled vesicle likely fuses with an unlabeled vesicle, and fluorescence consequently increases with fusion because of the larger separation between fluorescent and quenching lipids. This intervesicle lipid mixing correlates with lipid mixing that is sometimes assayed and observed in cell-cell fusion and which is a feature of steps of stalk formation and hemifusion for the fusion mechanism described in the Introduction. Specifically, stalk formation results in lipid mixing between the outer leaflets of the viral and target membranes, and hemifusion results in mixing between the inner leaflets of these membranes. FP_HM-induced vesicle fusion was typically nearly complete by t ≈ 600 s, and the associated fluorescence extent (F_{ext}) was approximately time-invariant. A 35 μL aliquot of 20% Triton X-100 detergent was then added and dissolved the vesicles, with consequent maximum fluorescence (F_{max}) associated with the large increase in separation between fluorescent and quenching lipids. By literature convention, time-dependent percent vesicle fusion is calculated as $M(t) = 100 \times [F(t) - F_0]/[F_{max} - F_0]$ with long-time fusion extent (M_{ext}) calculated using $F(t) = F_{ext}$. The $F \propto \langle 1/ [1 + (R_{For} / R)^6] \rangle$ where R is fluorophore/quencher distance, R_{For} is the Forster distance (~50 Å), and $\langle \ldots \rangle$ is the average over all fluorophores [71]. For the initial F_0 conditions, the estimated $\langle R \rangle \approx R_{For}$ and fusion between two vesicles results in $\langle R \rangle \approx (2)^{1/2} \times R_{For}$ with resulting $M_{ext} \approx 80\%$. There is typical 2% variation in M_{ext} for replicate assays using the same vesicle and FP_HM stocks [23]. Assays with different WT:V2E ratios were done on the same day using the same vesicle stock.

3. Results

3.1. Purified FP_HM

Fig. 2 displays SDS-PAGE of (A) WT and (B) V2E FP_HM at different stages of purification. The samples for the gel lanes had been solubilized in PBS and 8 M urea and were: (i) the cell pellet after removing PBS-soluble molecules; (ii) the precipitate formed in 300 mM NaCl; and (iii) the precipitate formed after the combined 300 and 600 mM imidazole elutions from the Co^{2+}-resin had been dialyzed against water. The (iii) lanes are the most important because this is the protein used in the subsequent experiments. Both WT and V2E exhibit a prominent band with apparent MW of ~15 kDa which was confirmed to be FP_HM by (C) anti-H_6 Western blot and by (Fig. S3) 88% coverage of the FP_HM sequence by peptides from trypsin digestion of the band. The preparation procedure for the Western blot has been previously described [33]. The 15 kDa band is observable in the (i) cell pellet lane for V2E and in the (ii) NaCl-induced precipitate for WT. When Co^{2+}-affinity purification was done without the NaCl precipitation, the elutions showed more impurities, particularly for WT. The yield after Co^{2+}-affinity purification was ~4 mg/L culture for WT and ~ 8 mg/L for V2E which correlates with a smaller cell pellet for WT vs. V2E. Relative to V2E, WT may be more fusion-active in the *E. coli* cells and have higher cytotoxicity.

3.2. WT is more helical than V2E and both proteins are hyperthermostable

Fig. 3 displays CD spectra of (A) WT and (B) V2E in Tris/SDS that were acquired between 22 and 95 °C. All spectra were acquired on a single day. At all temperatures, the WT and V2E spectra have a double-well shape that is characteristic of predominant helical structure. For WT at 22 °C, the magnitude of the mean-residue-molar-ellipticity at 222 nm ($|\theta_{222}|$) is 2.25×10^4 deg-cm^2-dmol^{-1}, which corresponds to 68% helicity using 3.3×10^4 deg-cm^2-dmol^{-1} for 100% helicity [72]. The

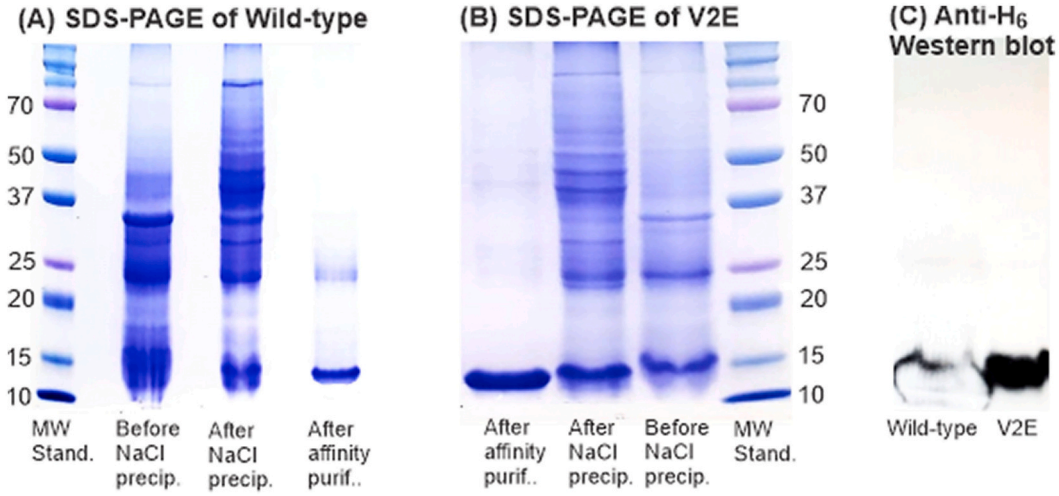

Fig. 2. SDS-PAGE at different steps of purification of (A) wild-type and (B) V2E FP_HM and (C) anti-H_6 western blotting of SDS-PAGE of both proteins after Co^{2+} affinity purification. The samples for the gel lanes had been solubilized in PBS and 8 M urea and were: (i) the cell pellet after removing PBS-soluble molecules; (ii) the precipitate formed in 300 mM NaCl; and (iii) the precipitate formed after the combined 300 and 600 mM imidazole elutions from the Co^{2+}-resin had been dialyzed against water.

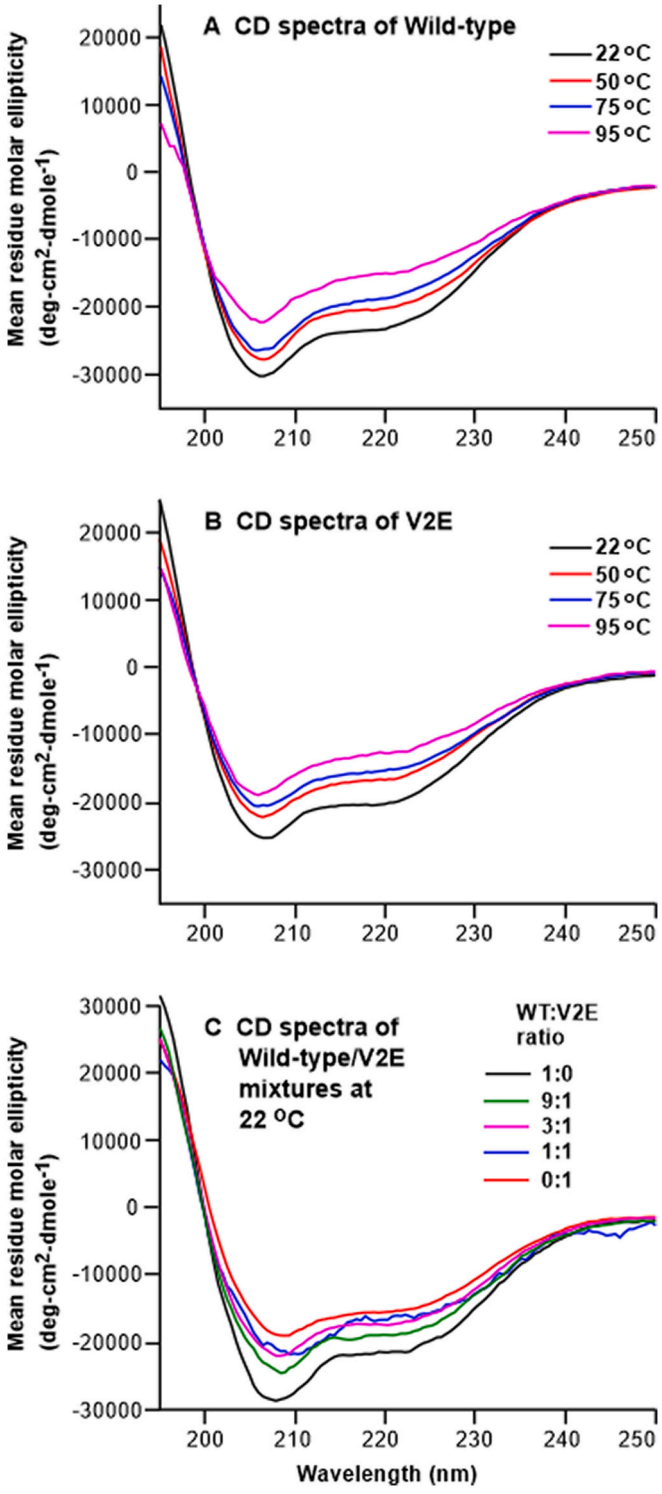

Fig. 3. Circular dichroism spectra of (A) Wild-type, (B) V2E, and (C) mixtures of Wild-type and V2E FP_HM. A sample typically contained [FP_HM] between 1 and 5 μM in 10 mM Tris at pH 7.4 with 0.2% SDS. The pure Wild-type and V2E samples in panels A and B were at temperatures between 22 and 95 °C. Spectra of replicate samples are displayed in Fig. S4. The mixtures in panel C were at 22 °C and were formed by co-dissolution in 8% SDS in which FP_HM is predominantly monomeric (Fig. 2A,B) followed by dialysis into 0.2% SDS to form mixed trimers (Fig. 4). All of the spectra in panels A-C are characteristic of predominant helical structure. The magnitude of the mean residue molar ellipticity at 222 nm ($|\theta_{222}|$) is the parameter typically used to quantitate helicity. At 22 °C, $|\theta_{222}|$ is ~15% smaller for (A) WT vs. (B) V2E and exhibits (C) V2E-dominant reduction in mixed WT/V2E trimers. The $|\theta_{222}|$ decreases with increasing temperature for both (A) WT and (B) V2E, but retains the wavelength-dependent profile that is characteristic of helical structure. These data evidence some helical disordering but not transformation to a random coil structure, and therefore $T_m > 95$ °C.

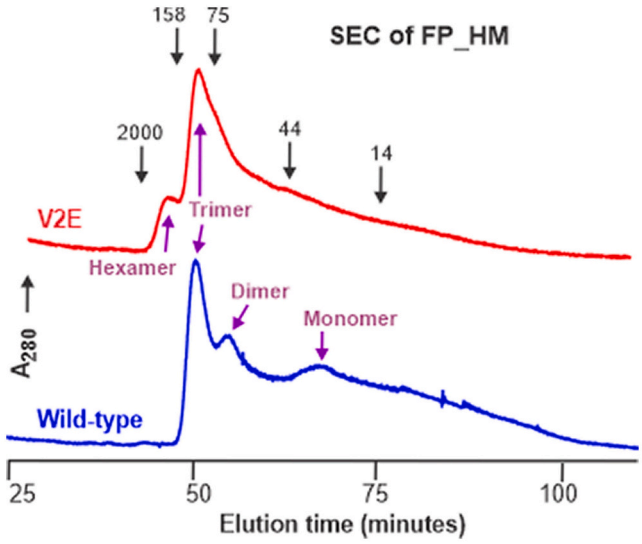

Fig. 4. Size-exclusion chromatography of FP_HM in 10 mM Tris at pH 7.4 with 0.2% SDS. There are (blue) Wild-type and (red) V2E traces. FP_HM at 1 mg/mL was loaded on a Superdex-75 column with ~10× dilution in running buffer and final A_{280} detection. Down-arrows mark the peak elution times of MW standards in kDa (Fig. S5). The MW's of peaks in the FP_HM traces were estimated by interpolation between MW standards using log(MW) dependence of elution time. The largest peak for both Wild-type and V2E is at ~90 kDa and assigned to FP_HM trimer with smaller peaks at ~160 kDa (hexamer) for Wild-type and ~ 70 kDa (dimer) and ~ 30 kDa (monomer) for V2E. The chromatograms are similar to earlier data for Wild-type but have broader peaks that may be due to absence of 150 mM NaCl in the running buffer for the present data and its presence for the earlier data. (For interpretation of the references to colour in this figure legend, the reader is referred to the web version of this article.)

68% value is very similar to the 66% helicity calculated using previous structural data. In particular, residues 23–70 and 117–164 are continuous N- and C-helices in crystal structures of hairpin constructs that are similar to HM [10]. Earlier CD and NMR studies support predominant β strand conformation for Fp residues, and non-helical structure is expected for the non-native SGGRGG loop and G_6LEH_6 tag [21,23–25].

For V2E at 22 °C, $|\theta_{222}| \approx 1.95 \times 10^4$ deg-cm^2-dmol^{-1}, which corresponds to 59% helicity. The reproducibility of greater WT vs. V2E helicity is evidenced by Fig. S4 CD spectra of FP_HM proteins from different purifications than in Fig. 3. The WT and V2E spectra between 50 and 95 °C are also consistent with predominant helical structure, but the |θ| values become smaller as temperature increases, with $|\theta_{222}|_{95C}/|\theta_{222}|_{22C} \approx 2/3$ for spectra of all WT and V2E samples. The CD spectra support $T_m > 95$ °C for WT and V2E, which is consistent with the previously-reported WT $T_m \approx 110$ °C from differential scanning calorimetry [43,44].

3.3. WT and V2E are predominantly trimeric in Tris/SDS

Earlier studies showed there can be many different oligomeric states of gp41 hairpin constructs in aqueous solution, including monomer, dimer, trimer, hexamer, and dodecamer [22,25,33,37,73,74]. The distribution of oligomeric states depended on the gp41 regions in the construct, concentration of the construct, and additives and pH in the solution. For the present study, the distribution of oligomeric states in Tris/SDS at pH 7.4 was studied because earlier SEC showed predominant trimers for WT in this environment, and hairpin trimers may be the fusion-active state of gp41 [25]. Fig. 4 displays the SEC profiles for WT and V2E, with down arrows marking the positions of peaks of MW standards. Fig. S5 displays the SEC profiles for these standards. The dominant SEC peak for WT and V2E has apparent MW ≈ 90 kDa which was calculated using interpolation between MW standards and $K_{av} \propto \log$ (MW). This was also the dominant peak in the earlier WT SEC and is assigned as the trimer [25]. There is a smaller peak for V2E with MW ≈ 165 kDa that is assigned as the hexamer, and smaller peaks for WT with MW ≈ 70 kDa and 35 kDa that are respectively assigned as dimer and monomer. Peaks with similar masses as the assigned species have been observed in earlier SEC of FP_HM and HM in DPC detergent at pH 4 [25]. The monomer, dimer, trimer, and hexamer assignments correlate with SDS mass contributions of ~20, 35, 40, and 65 kDa, respectively. It is likely that most of the SDS molecules bind the apolar Fp and Mper segments of FP_HM. The mass of these segments is ~3 kDa per FP_HM molecule, and the SDS:Fp + Mper mass ratios with these assignments are within the previously-reported range of 3–7 for SDS-bound membrane protein segments [75].

We chose Tris/SDS as the buffer of stock FP_HM for vesicle fusion assays, based on predominant folded helical trimer for WT and V2E (Figs. 3 and 4), and the likelihood that this is an important catalytic structure of gp41 during fusion. Although some proteins unfold in SDS and others adopt increased helical structure, neither of these effects are apparent in the Figs. 3 and 4 data. As noted above, the θ_{222} of WT in SDS at 22 °C matches the fractional helicity calculated using the lengths of helical segments of the crystal structure of a HM-like construct. The crystal was grown in the absence of detergent [10]. Also, the Fig. 3 CD spectra of (A) WT and (B) V2E support $T_m > 95$ °C, which is consistent with $T_m \approx 110$ °C detected for FP_HM and similar constructs in the absence of detergent [25,44]. In addition, earlier crystal structures and CD studies of gp41 constructs that are smaller than FP_HM show either no change or small increase or decrease in helicity with vs. without detergent, where SDS was sometimes the detergent [24,76].

3.4. FP_HM induces highest vesicle fusion extent near pH 5 with much greater fusion for WT vs. V2E

Fig. 5 displays vesicle fusion induced by WT and V2E in the pH range of 3.3–7.4 and with FP_HM:lipid = 1:100 mol ratio. For all pH's, WT induces greater fusion extent (M_{ext}) than V2E. For both WT and V2E, M_{ext} exhibits a maximum at pH 5.3 with lower extents at lower and higher pH. This is different than an earlier study for similar gp41 constructs which showed monotonic decrease in fusion extent as pH was raised from 3.5 to 7 [45]. These different dependences of fusion extent vs. pH may be related to the initial protein trimer state for the present study vs. predominant monomer state in the earlier study [33]. For the present study, the initial rate of fusion is inversely correlated with pH, which was also observed in an earlier study [23]. In addition, the $M_{ext,WT}/M_{ext,V2E}$ ratio becomes larger as pH is increased. This trend is most apparent by comparing pH 4.3 and 6.3 data which both have $M_{ext,WT} \approx$ 30% whereas $M_{ext,V2E} \approx$ 17% at pH 4.3 and 7% at pH 6.3. Subsequent assays were done at pH 5.3 where fusion is maximal.

3.5. Mixed WT/V2E trimers exhibit V2E-dominant reduction of vesicle fusion and helicity

There has been 30-year interest in the striking gp41 V2E-dominant reduction of gp160-induced cell/cell fusion and HIV infection. These data have been analyzed to estimate the number of gp160 trimers required for fusion and infection. We tested whether there are also V2E-dominant reductions of FP_HM-induced vesicle fusion and helicity. These experiments required mixed WT/V2E trimers, so WT and V2E were first co-dissolved in SDS-PAGE buffer in which both proteins are predominantly monomeric (Fig. 2) and then dialyzed into Tris/SDS in which the proteins are predominantly trimeric (Fig. 4). Fig. 6 displays vesicle fusion with FP_HM:lipid = 1:100 and different WT:V2E ratios and Fig. 3C displays CD spectra with different WT:V2E ratios. Both datasets demonstrate that V2E causes dominant reductions of fusion and helicity. The V2E dominance is supported by fusion data obtained with WT and V2E stocks from other purifications and by data with FP_HM:lipid = 1:300 (Fig. S6). The fusion extents for all data are presented in

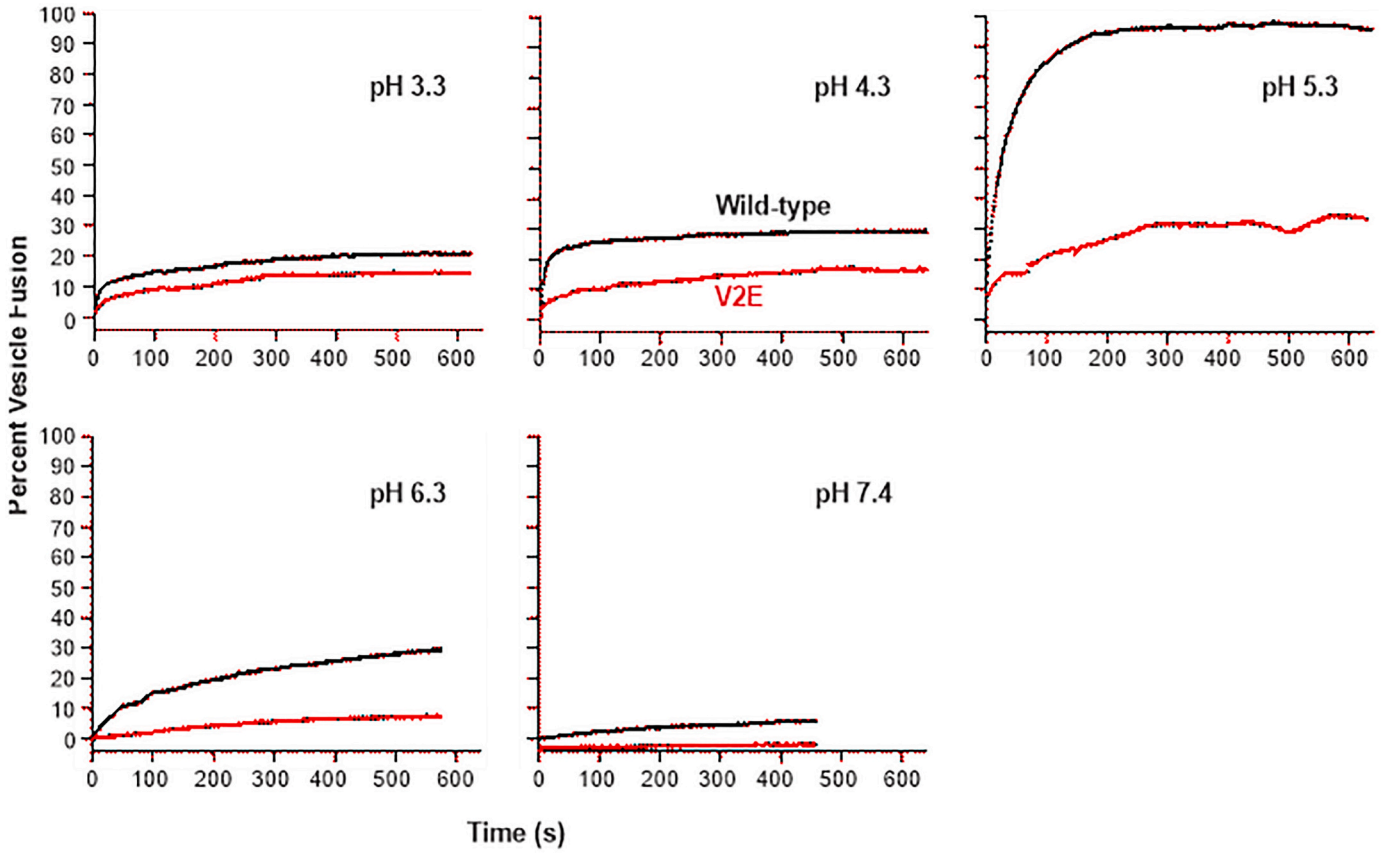

Fig. 5. Vesicle fusion induced by Wild-type (black) and V2E mutant (red) FP_HM at pH's between 3.3 and 7.4. Assays were done at 37 °C using vesicles that had been extruded through 100 nm diameter pores. The vesicles contained POPC:POPG (4:1) with [total lipid] = 150 μM. The vesicle solution contained 25 mM citrate buffer at pH = 3.3, 4.3, 5.3, and 6.3, and 10 mM Tris buffer at pH = 7.4. At time = 0, an aliquot of FP_HM stock solution was added to the vesicle solution to achieve FP_HM: lipid with 1:100 M ratio. The stock had 150 μM FP_HM at pH 7.4 with 0.2% SDS. The small apparent negative fusion for V2E at pH 7.4 is likely the result of fluorophore dilution because of increased volume of the vesicle solution upon addition of FP_HM stock. (For interpretation of the references to colour in this figure legend, the reader is referred to the web version of this article.)

Table 1.

3.6. Quantitative similarity of V2E dominance for FP_HM fusion and helicity, gp160 cell-cell fusion, and HIV infectivity, and global fitting support efficient fusion requiring at least two Wild-type gp41 trimers

It is interesting to understand how quantitatively-similar are the V2E dominances for FP_HM-induced vesicle fusion, FP_HM helicity, gp160-induced cell/cell fusion, and HIV infectivity [54]. For each assay type, percent activity (A) is calculated as a function of the fraction gp41 with V2E (f_{V2E}), with A = 100% and 0% when f_{V2E} = 1 and 0, respectively. For cell/cell fusion and infectivity, $A = 100 \times N(f_{V2E})/N(0)$, were N = experimental numbers of syncytia and colonies, respectively. For f_{V2E} = 0.5, the A's are ~0, which presumably also holds for f_{V2E} = 1. For FP_HM-induced vesicle fusion, the $A(f_{V2E}) = 100 \times [M_{ext}(f_{V2E}) - M_{ext}(1)]/[M_{ext}(0) - M_{ext}(1)]$, and a similar expression is used for FP_HM helicity with θ_{222} substituted for M_{ext}. Table 2 displays the A values from the different assays and their associated uncertainties and Fig. 7 displays a plot of all A vs. f_{V2E}. A straightforward model for V2E dominance is that activity requires a cluster with number ≡ n WT gp41 molecules, so activity is proportional to the fraction of these clusters with only WT and without V2E gp41 molecules. For this model, $A = 100 \times (f_{WT})^n = 100 \times (1 - f_{V2E})^n$. Global fitting of all the Fig. 7 data yields best fit $n = 6.00 \pm 0.39$, i.e. $T = 2$ fully WT trimers are required for the greatest cell-cell and vesicle fusion, HIV infection, and helical hairpin structure.

4. Discussion

4.1. V2E dominance of FP_HM vesicle fusion and helicity supports an important role of the final gp41 hairpin structure in maintaining close membrane apposition prior to fusion

The V2E mutation of gp41 exhibits dominance in both gp160-mediated cell/cell fusion and HIV infectivity [54]. Several different groups have analyzed infectivity data as a function of f_{V2E} with resulting estimates between 1 and 19 gp160 trimers required for infection, with the specific number depending on the assumptions of the model used in the analysis [55]. The major discovery of the present study is V2E dominance for FP_HM in both vesicle fusion and helicity that is quantitatively-similar to earlier cellular and viral data (Table 2 and Fig. 7). FP_HM adopts the hyperthermostable trimer-of-hairpins structure which is the final state of gp41 without gp120, so this similar dominance supports an important role in viral fusion for the final hairpin structure. These data do not support models in which the hairpin is the "post-fusion" structure that forms after most or all of membrane fusion has occurred. Fig. 8 displays a model that correlates the reductions in gp41 helicity and fusion for V2E vs. WT hairpin gp41. Panel A depicts two WT trimers ($n = 6$, $T = 2$) whose hairpins have ~60-residue N- and C-helices, with trimers connected through an antiparallel β sheet located in the outer leaflet of the target membrane and composed of six interleaved Fp strands, each with ~17 N-terminal gp41 residues. For clarity, only a single molecule of each trimer is displayed. The hyperthermostability of the hairpin ($T_m \approx 110$ °C), in conjunction with the Fp

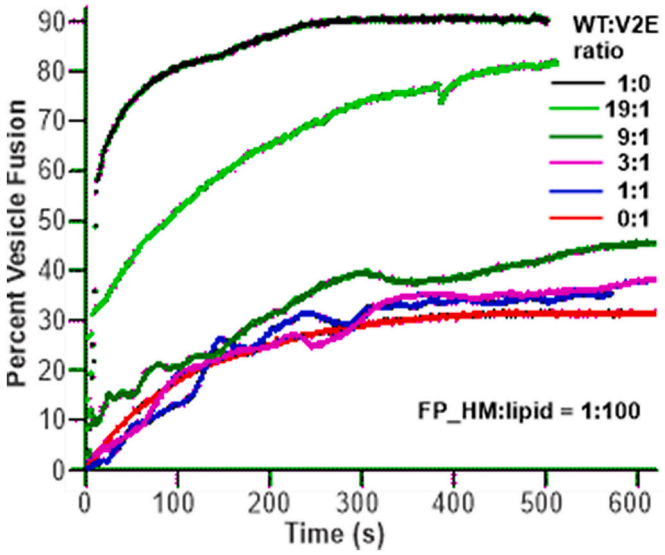

Fig. 6. Vesicle fusion induced by FP_HM mixed trimers with different Wild-type:V2E ratios. The vesicle solution had 150 μM total lipid, pH 5.3, temperature = 37 °C, and POPC:POPG (4:1) vesicles formed by extrusion through 100 nm diameter pores. At time = 0, an aliquot of FP_HM stock solution was added to the vesicle solution to achieve FP_HM:lipid = 1:100 M ratio. The stock had 150 μM FP_HM at pH 7.4 with 0.2% SDS. Stocks with Wild-type/V2E mixtures were prepared by co-dissolution in 8% SDS with predominantly monomeric FP_HM (Fig. 2 A,B) followed by dialysis into 0.2% SDS to form FP_HM mixed trimers (Fig. 4). Fig. S8 displays vesicle fusion data with different preparations of vesicles and protein stocks, and with FP_HM:lipid either 1:100 or 1:300. The data in Fig. 5 and Fig. S8 data exhibit similar trends and the long-time fusion extents are presented in Table 1. The fusion extent is <1% when stock buffer without FP_HM is added to the vesicle solution.

Table 1
Percent Fusion Extent for different V2E mole fractions.[a]

f_{V2E}	Protein: Lipid = 1:100 (Dataset 1)	Protein: Lipid = 1:100 (Dataset 2)	Protein: Lipid = 1:300
0	90	96	43
0.05	81	86	32
0.10	48	65	25
0.25	38	44	15
0.5	35	31	15
1	32	30	18

[a] Data for each column were obtained using a separate vesicle preparation and a separate protein stock preparation. The $M_{ext} = 100 \times (F_{ext} - F_0)/(F_{max} - F_0)$ where F_0 is the fluorescence prior to protein addition, F_{ext} is the long-time (~600 s) asymptotic fluorescence after protein addition, and F_{max} is the maximum fluorescence after Triton X-100 addition. There is typical ±2% variation in M_{ext} for an assay replicate with the same vesicle preparation and same protein stock preparation.

in target membrane and Mper+Tmd in viral membrane, partially counteracts the ~25 kcal/mol energy for close membrane apposition prior to fusion. The energy for this initial apposition is the highest barrier in many computational studies of membrane fusion [4]. For the Fig. 8A model, the final trimer-of-hairpins state is the fusion-catalytic state of gp41 and forms prior to fusion, which is consistent with the results of some earlier experiments and simulations of enveloped virus fusion [46,47]. The N-helix and C-helix in Fig. 8A are approximately residues 24–84 and 104–164, respectively, based on high-resolution structures and supported by the WT CD spectra in Fig. 3A, as described in the Results section [9,10]. Two trimers for efficient fusion is supported by fitting of the Activity vs. f_{V2E} data (Fig. 7 and Table 2) and agrees semi-quantitatively with an earlier report of two to three gp160

Table 2
Percent activity for different V2E mole fractions.[a]

f_{V2E}	Vesicle fusion P:L = 1:100 (Dataset 1)	Vesicle fusion P:L = 1:100 (Dataset 2)	Vesicle fusion P:L = 1:300	Helicity	Cell-cell fusion	HIV infectivity
0.05	85(6)	85(6)	58(13)			
0.09					39(20)	44(4)
0.10	27(5)	54(5)	30(12)	56(5)		
0.17					18(8)	33(10)
0.25	11(5)	22(4)		28(5)		
0.33					6(1)	16(4)
0.5	6(5)	2(1)		11(5)	4(3)	5(2)

[a] For FP_HM-induced vesicle fusion and FP_HM helicity, Activities (A's) were based on the present study, and for cell-cell fusion and HIV infectivity, on [54]. Uncertainties are in parentheses. For vesicle fusion, $A(f_{V2E}) = 100 \times \{[M_{ext}(f_{V2E}) - M_{ext}(1)]/[M_{ext}(0) - M_{ext}(1)]\}$. The uncertainty of A was calculated using ±2% uncertainty for each M_{ext}. The helicity A was similarly calculated with θ_{222} substituted for M_{ext}. Cell-cell fusion was done with HeLa T4 cells transfected with plasmids coding for the HIV gp160 protein, and f_{V2E} was a fraction of the transfected DNA. Fusion was quantified using the number of cellular syncytia (N), with $A = 100 \times \{N(f_{V2E})/N(0)\}$. The uncertainty of A was the standard deviation from several trials. HIV infectivity was similarly quantified with N = number of colonies after infection and incubation of HeLa T4 cells.

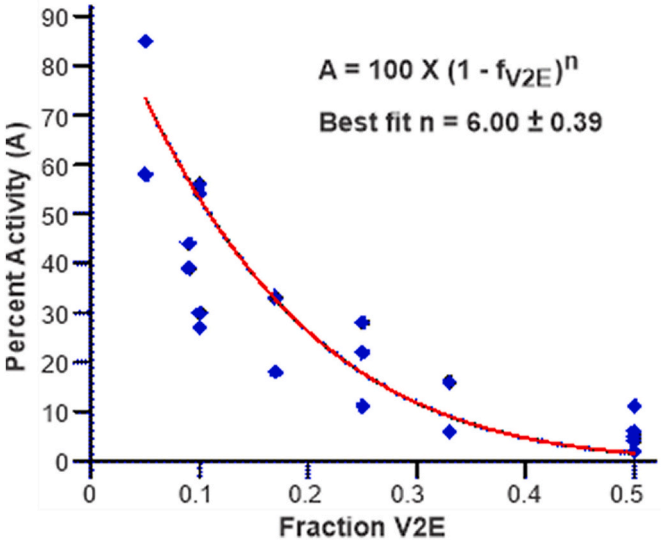

Fig. 7. Plot of Percent Activity (A) vs. fraction V2E (f_{V2E}) data and fitting to $A = 100 \times (1 - f_{V2E})^n$. The individual A values and their uncertainties are presented in Table 2 and are based on vesicle fusion and circular dichroism data from the present study and earlier cell-cell fusion and HIV infection data. The fitting equation is based on fusion requiring n Wild-type and no V2E molecules. The best-fit $n = 6.00 \pm 0.39$, i.e. 6.00(39). For data subsets from a single approach where f_{V2E} is the only variable parameter (single columns in Table 2), best-fit n are: FP_HM-induced vesicle fusion at 1:100 ratio, trial 1, 8.68(2.36) and trial 2, 5.29(41); FP_HM-induced vesicle fusion at 1:300 ratio, 11.10(40); CD-calculated FP_HM helicity, 4.69(65); gp160-induced cell-cell fusion, 7.14 (40); and HIV infectivity, 6.97(1.49).

trimers for efficient infection by HIV primary isolates, i.e. HIV strains obtained from infected patients [55]. One of these isolates was a "transmitted founder" isolate, i.e. an isolate that initiates infection of an uninfected person. In Fig. 8, the Fp antiparallel β sheet structure in membrane is supported by NMR data which also show a distribution of N-terminal strand lengths, with 1 → 17/17 → 1 as a major population [18–20]. This registry clusters together the apolar N-terminal Fp

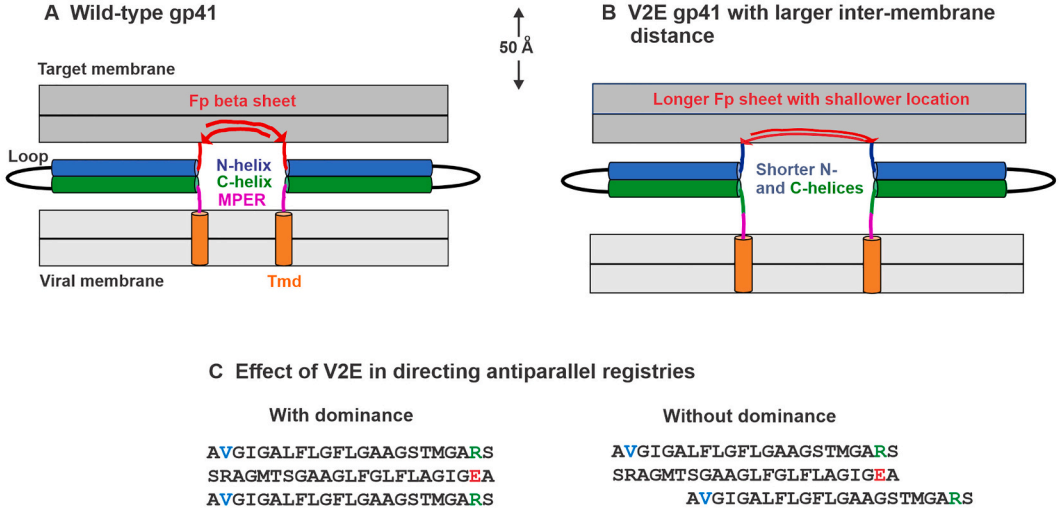

Fig. 8. (A, B) Model that correlates lower helicity of V2E vs. Wild-type FP_HM with reduced fusion of V2E. The gp41 hairpin reduces the energy of the membrane apposition state that exists just prior to fusion. There are two gp41 trimers with hairpin structure that are joined through an intermolecular Fp β sheet in the outer leaflet of the target membrane. The Fp strands are antiparallel and interleaved between trimers. For clarity, only one gp41 monomer is shown in each trimer. The model has dominant C-terminal extension of the Fp β sheet for V2E vs. Wild-Type that results in loss of helicity at the N-terminus of the N-helix and C-terminus of the C-helix. There is consequent larger separation of the viral and target membranes for V2E and higher activation barrier for subsequent stalk formation because of the need for larger-amplitude protrusion of lipid acyl chains into the intermembrane region. Relative to WT, the V2E Fp β sheet may also have shallower membrane location with consequent lower probability of lipid protrusion. For (A) Wild-type gp41 hairpin, the N- and C-helices are each ~60 residues. There is a distribution of WT Fp antiparallel registries that includes residues 1 → 17/17 → 1 which is depicted in panel A and in panel C, right, V2E middle strand/WT bottom strand. This registry clusters together the apolar N-terminal Fp residues of the different strands which likely correlates with more favorable free energy of insertion in the membrane hydrophobic core. A longer 1 → 23/23 → 1 registry is depicted for V2E in panel B, and correlates with loss of 6 helical residues in both the N- and C-helices and the experimentally-observed ~9% loss of helicity for V2E vs. WT FP_HM (Fig. 3A,B). This registry is depicted in panel C, left and could correlate with an interstrand E2/R22 salt bridge. The membrane thickness and lengths and widths of the N- and C-helices and Tmd in panels A and B are drawn approximately to the displayed scale. Helices are drawn with ~1.5 Å length per residue, Fp β strands are drawn with ~3.5 Å length per residue, and other gp41 segments are drawn with ~2.5 Å length per residue. The Mper may also bind the viral membrane, based on existing Mper structures. Panel C displays schematic registry arrangements of three antiparallel Fp strands, WT/V2E/WT either (left) with or (right) without V2E dominance of registries, i.e. 1 → 23/23 → 1/1 → 23 or 1 → 23/23 → 1/1 → 17.

residues of the different strands which likely correlates with more favorable free energy of insertion into the membrane hydrophobic core (Fig. 8C, right panel, middle and bottom strands). Although FP_HM doesn't have the Tmd, its C-terminal Mper also binds membrane, and intervesicle lipid mixing could be catalyzed by FP_HM by a similar structure as shown for the Fig. 8A fusion catalyzed by full-length gp41 with Tmd [26,27].

Fig. 8B displays a model with the V2E gp41 hairpin, and reduced fusion is predominantly attributed to the larger membrane separation for V2E vs. WT. The Fp β sheet in V2E is hypothesized to have longer strands, e.g. 1 → 23, because of salt bridge formation and/or hydrogen bonding between the E2 sidechain and sidechains of polar residues in the Fp C-terminal region, e.g. R22 (Fig. 8C) [20]. The longer and perhaps more stable Fp β sheet for V2E vs. WT may also be the basis for the observed minor hexamer population for V2E in SDS vs. minor dimer and monomer populations for WT (Fig. 4). The β sheet structure has been previously observed for V2E peptide in membrane, and there are conflicting data about whether there is greater fractional population of helical or β sheet structure for V2E vs. WT peptides [61,62,64]. NMR data support predominant β sheet structure for the Fp segment of a membrane-bound construct similar to WT FP_HM [23]. Given that the present study for FP_HM shows lower helicity for V2E vs. WT (Fig. 3A,B and Fig. S4A,B) as well as V2E-dominant reduction in helicity for WT:V2E mixtures (Fig. 3C), our Fig. 8 model uses the V2E β sheet structure. Longer V2E vs. WT β sheets are supported by some comparative NMR data for V2E vs. WT peptides in membrane [20]. These data also support a distribution of antiparallel registries for V2E as has been observed for WT, but for clarity the following discussion is focused on the 1 → 23/23 → 1 V2E antiparallel registry. For WT, residues 18–23 are the linker that connects the Fp β sheet in the target membrane and the hairpin N-helix in the intermembrane region. For V2E, the linker would instead be residues 24–29 which in WT form the N-terminus of the N-helix. These residues are no longer helical in V2E, and as a consequence, no longer stabilize the helical structure of six residues at the C-terminus of the C-helix. The loss of helicity for 12 hairpin residues for V2E vs. WT approximately matches the experimental ~9% loss in helicity for V2E vs. WT FP_HM (Fig. 3A,B), i.e. 0.09 × 146. The loss of helicity for the C-helix residues results in a ~ 10 Å increase in intermembrane separation with consequent reduction in fusion. Specifically, the stalk intermediate between outer leaflets of the viral and target membranes is hypothesized to form after apposition via transient "protrusion" (excursion) of lipid acyl chains into the aqueous phase [47–50]. For the larger separation with V2E, stalk formation would require larger-amplitude and therefore higher energy protrusion of the chains, and fusion would be hindered. Earlier NMR studies also showed that relative to membrane without Fp, membrane with WT Fp exhibits increased chain protrusion [50]. Other NMR data showed that the V2E Fp β sheet membrane location is shallower than WT, and this difference may result in attenuated protrusion with V2E gp41 [64].

4.2. Interleaved fusion peptide strands from two gp41 trimers in an antiparallel β sheet structure as the basis for V2E dominance

In our view, there hasn't yet been a detailed structural model that explains V2E dominance in HIV fusion and infection, and this intellectual gap is addressed by the Fig. 8 model with antiparallel β sheet with interleaved Fp strands from two trimers. Fig. 8C displays schematic registry arrangements of three antiparallel strands, WT/V2E/WT either (left) with or (right) without V2E dominance of registries, i.e. 1 → 23/23 → 1/1 → 23 or 1 → 23/23 → 1/1 → 17, respectively. The (left) dominant arrangement might be favored because a R22/E2 salt bridge can form either between the top/middle or bottom/middle strands. If

two or three of the six strands in the sheet are V2E, there would be even higher preference for the 1 → 23/23 → 1 registry. For $f_{V2E} = 0.5$, the maximum number of R22/E2 salt bridges would be achieved when alternating WT and V2E strands only adopt the 1 → 23/23 → 1 registry. The predicted absence of fusion and infection with only 1 → 23/23 → 1 registry matches the calculated A = 2% when $f_{V2E} = 0.5$ using the best-fit eq. $A = 100 \times (1 - f_{V2E})^6$, Fig. 7. Our model of V2E-dominant reduction in fusion and helicity caused by V2E-dominant longer Fp strand lengths includes the reasonable idea that larger intermembrane separation and perhaps shallowness of membrane location of the Fp β sheet are positively-correlated with the number of 1 → 23/23 → 1 registries within the sheet.

4.3. Comparison between the gp41 V2E and Ha2 G1E fusion-impairing mutations

The Fig. 8 correlation between increased membrane separation and reduced fusion is also evidenced by the similar structural effects of impairing mutations for the influenza Ha2 protein which catalyzes fusion for this virus. Ha2 and gp41 don't share sequence homology but have similar topologies including a viral Tmd and a ~ 180 residue ectodomain that adopts a final-state trimer-of-hairpins structure [77,78]. Like gp41, Ha2 also has a ~ 25-residue N-terminal Fp that binds the target membrane. However, the Ha2 Fp typically adopts helical rather than β sheet structure in membrane and there isn't close spatial proximity between the helical Fp's of the same or different trimers [69,79–81]. Two extensively-studied Ha2 mutations are I173E in the C-terminal region of the hairpin close to the Tmd, and G1E at the N-terminus of the Fp. Both the I173E and G1E mutations greatly reduce Ha-mediated cell/cell fusion, and also greatly reduce cell-cell fusion mediated by the Ha2 ectodomain protein "FHa2" which is analogous to FP_HM [46,82,83]. Vesicle fusion induced by FHa2 is also highly attenuated with these mutations which is similar to the attenuation of vesicle fusion by V2E FP_HM (Fig. 5) [81]. Unlike V2E (Fig. 3A,B), both I173E and G1E cause dramatic 35–40 °C reductions in the T_m of FHa2, so the loss of fusion with either mutation is correlated with less stable hairpin and with larger inter-membrane separation [81]. The reduction in T_m for G1E is surprising because the N-terminus of the WT helical Fp is spatially far from the hairpin. However, H/D exchange data of Ha2 supports a model for reduced hairpin stability in which G1E Fp binding to the C-terminal region of the hairpin displaces the N-helix from the hairpin [78]. G1E may not be a dominant Ha2 mutation, as each Fp adopts independent helical structure [69,80]. To our knowledge, G1E dominance has not been reported for Ha2 fusion.

4.4. Greatest fusion between pH 5 and 6 is correlated with retention of FP_HM trimers

Observation of maximum vesicle fusion between pH 5 and 6 for both WT and V2E (Fig. 5) is different from an earlier study which found maximum fusion at pH ≈ 3 and decreasing fusion as pH is raised, with negligible fusion when pH is in the 5–6 range [45]. The construct of the earlier study was similar to WT FP_HM and similar lipid compositions were used for vesicles in both studies, with a minor fraction of POPG lipid that has negative headgroup charge over the entire pH range. One difference between studies is the stock protein buffer which was formate at pH 3 in the earlier study vs. Tris/SDS at pH 7.4 in the present study. For both buffers, the stock protein is a thermostable hairpin with $T_m >$ 100 °C; however, the protein is predominantly a monomer at pH 3 vs. trimer at pH 7.4 [25,33]. This pH-dependent difference is consistent with the calculated charges of ≈ +12 at pH 3 vs. -1 at 7.4, and the consequent much larger electrostatic repulsive energy between monomer units at pH 3. At pH 7.4, vesicle fusion is induced by the stock trimer (Fig. 5) but is not induced by the stock monomer in the earlier study. We anticipate the stock trimer remains intact because the pH doesn't change. Although the stock monomer could form the lowest free-energy trimer at pH 7.4, a significant fraction of protein likely binds vesicles as monomers and wouldn't adopt the interleaved FP β sheet structure from two trimers, so there is less compensation of the 25 kcal/mol apposition barrier and consequent attenuated fusion (Fig. 8A).

For the present study, fusion was measured in the pH 3.3–7.4 range and the maximum extent of fusion was observed between pH 5 and 6 (Fig. 5). Based on the discussion above, the FP_HM oligomeric state may be an important factor in the pH dependence. An earlier study provides insight into the pH dependence of FP_HM oligomerization, and relied on analytical ultracentrifugation data in dodecylphosphocholine (DPC) detergent of a construct containing FP_HM plus the transmembrane domain [84]. There was predominant monomer at pH 4, predominant trimer at pH 6, and approximately equal fractions of monomer and trimer at pH 5. Another earlier study showed greater trimer vs. monomer for FP_HM in SDS vs. DPC so we anticipate FP_HM remains a trimer at pH 5.3 where fusion extent is maximal [25]. The more extensive fusion for FP_HM at pH 5.3 vs. higher pH may be due to the +2 charge at pH 5.3 vs. neutral or negative charge at higher pH, with consequent greater FP_HM binding to the negatively-charged membrane at pH 5.3 [23,33]. The lower fusion when pH < 5 may be due to FP_HM dissociation into monomers which are probably less fusion-active than trimer. It isn't yet known whether the maximum FP_HM-induced vesicle fusion in the pH 5–6 range is related to HIV fusion within endosomes in this pH range. Fusion within late endosomes is the major infection route for some viruses like influenza, but for HIV there is disagreement in the literature about whether infection is primarily via fusion with the plasma membrane or within endosomes [85–87].

5. Conclusions

The most important result of this study is observation of V2E mutational dominance in reduction of helicity and vesicle fusion induced by FP_HM, which is a hyperthermostable HIV gp41 hairpin construct that includes the Fp and Mper that bind the target and viral membranes, respectively. This mutation had previously been observed to be dominant in reduction of gp160-mediated cell/cell fusion and HIV infection. Both FP_HM and gp160 are predominantly trimers prior to fusion and infection, and mixed trimers with WT and V2E molecules exhibit quantitatively-similar dependences of reduced helicity, fusion, and infection on f_{V2E}. Our observation of similar V2E dominance for FP_HM and gp160 supports the final trimer-of-hairpins structure of gp41 as an important state in fusion catalysis. A global fit of the present and earlier V2E data supports efficient fusion and infection requiring 6 WT gp41 molecules, i.e. two gp41 trimers. A model is developed with two gp41 hairpin trimers stabilizing the highest-energy initial apposition of the viral and target membranes prior to fusion. The Mper/Tmd's are in the viral membrane and the Fp's are in the target membrane with intermolecular antiparallel β sheet structure and interleaved strands from the two trimers. The hyperthermostable hairpins in conjunction with the Fp in target membrane and Mper/Tmd in viral membrane reduce the membrane apposition energy and thereby catalyze fusion. There are longer Fp strands in V2E vs. WT which results in loss of helicity for V2E at the N- and C-termini of the hairpin and consequent larger intermembrane separation. Subsequent formation of the stalk membrane intermediate is impaired with larger separation because of the need for higher-amplitude and therefore higher-energy protrusion of lipid acyl chains into the aqueous region. The V2E dominance of longer strands in the Fp β sheet is correlated with formation of stabilizing salt bridges and/or hydrogen bonds between E2 and the polar and charged residues near the Fp C-terminus.

CRediT authorship contribution statement

Md Rokonujjaman: Methodology, Validation, Formal analysis, Investigation, Resources, Data curation, Writing – original draft, Visualization, Supervision, Funding acquisition. **Abdulrazak Sahyouni:**

Investigation, Resources. **Robert Wolfe:** Methodology, Resources, Supervision. **Lihui Jia:** Methodology, Validation, Investigation, Resources. **Ujjayini Ghosh:** Resources, Supervision. **David P. Weliky:** Conceptualization, Methodology, Formal analysis, Data curation, Writing – original draft, Writing – review & editing, Visualization, Supervision, Project administration, Funding acquisition.

Declaration of Competing Interest

The authors declare that they have no known competing financial interests or personal relationships that could have appeared to influence the work reported in this paper.

Data availability

Data will be made available on request.

Acknowledgements

This work was supported by the National Institutes of Health grant number R01 AI047153. DNA sequencing and trypsin digestion and peptide mass spectrometry analyses were done by the MSU Genomics and Proteomics facilities.

Appendix A. Supplementary material

DNA sequences of FP_HM and primers used to produce V2E mutation; Proteomics sequence coverage; Replicate temperature-dependent CD spectra; SEC of MW standards; Vesicle fusion at different peptide: lipid ratios. Supplementary data to this article can be found online at [https://doi.org/10.1016/j.bpc.2022.106933].

References

[1] R. Blumenthal, M.J. Clague, S.R. Durell, R.M. Epand, Membrane fusion, Chem. Rev. 103 (2003) 53–69.
[2] J.M. White, S.E. Delos, M. Brecher, K. Schornberg, Structures and mechanisms of viral membrane fusion proteins: multiple variations on a common theme, Crit. Rev. Biochem. Mol. Biol. 43 (2008) 189–219.
[3] R. Blumenthal, S. Durell, M. Viard, HIV entry and envelope glycoprotein-mediated fusion, J. Biol. Chem. 287 (2012) 40841–40849.
[4] S. Boonstra, J.S. Blijleven, W.H. Roos, P.R. Onck, E. van der Giessen, A.M. van Oijen, Hemagglutinin-mediated membrane fusion: a biophysical perspective, Ann. Revs. Biophys. 47 (2018) 153–173.
[5] L.V. Chernomordik, M.M. Kozlov, Mechanics of membrane fusion, Nat. Struct. Mol. Biol. 15 (2008) 675–683.
[6] M. Pancera, T.Q. Zhou, A. Druz, I.S. Georgiev, C. Soto, J. Gorman, J.H. Huang, P. Acharya, G.Y. Chuang, G. Ofek, G.B.E. Stewart-Jones, J. Stuckey, R.T. Bailer, M. G. Joyce, M.K. Louder, N. Tumba, Y.P. Yang, B.S. Zhang, M.S. Cohen, B.F. Haynes, J.R. Mascola, L. Morris, J.B. Munro, S.C. Blanchard, W. Mothes, M. Connors, P. D. Kwong, Structure and immune recognition of trimeric pre-fusion HIV-1 Env, Nature 514 (2014) 455–461.
[7] A.B. Ward, I.A. Wilson, The HIV-1 envelope glycoprotein structure: nailing down a moving target, Immunol. Rev. 275 (2017) 21–32.
[8] M. Caffrey, M. Cai, J. Kaufman, S.J. Stahl, P.T. Wingfield, D.G. Covell, A. M. Gronenborn, G.M. Clore, Three-dimensional solution structure of the 44 kDa ectodomain of SIV gp41, EMBO J. 17 (1998) 4572–4584.
[9] Z.N. Yang, T.C. Mueser, J. Kaufman, S.J. Stahl, P.T. Wingfield, C.C. Hyde, The crystal structure of the SIV gp41 ectodomain at 1.47 A resolution, J. Struct. Biol. 126 (1999) 131–144.
[10] V. Buzon, G. Natrajan, D. Schibli, F. Campelo, M.M. Kozlov, W. Weissenhorn, Crystal structure of HIV-1 gp41 including both fusion peptide and membrane proximal external regions, PLoS Pathog. 6 (2010) e1000880.
[11] S.R. Durell, I. Martin, J.M. Ruysschaert, Y. Shai, R. Blumenthal, What studies of fusion peptides tell us about viral envelope glycoprotein-mediated membrane fusion, Mol. Membr. Biol. 14 (1997) 97–112.
[12] R. Kong, K. Xu, T.Q. Zhou, P. Acharya, T. Lemmin, K. Liu, G. Ozorowski, C. Soto, J. D. Taft, R.T. Bailer, E.M. Cale, L. Chen, C.W. Choi, G.Y. Chuang, N.A. Doria-Rose, A. Druz, I.S. Georgiev, J. Gorman, J.H. Huang, M.G. Joyce, M.K. Louder, X.C. Ma, K. McKee, S. O'Dell, M. Pancera, Y.P. Yang, S.C. Blanchard, W. Mothes, D. R. Burton, W.C. Koff, M. Connors, A.B. Ward, P.D. Kwong, J.R. Mascola, Fusion peptide of HIV-1 as a site of vulnerability to neutralizing antibody, Science 352 (2016) 828–833.
[13] M.J. van Gils, T.L.G.M. van den Kerkhof, G. Ozorowski, C.A. Cottrell, D. Sok, M. Pauthner, J. Pallesen, N. de Val, A. Yasmeen, S.W. de Taeye, A. Schorcht, S. Gumbs, I. Johanna, K. Saye-Francisco, C.-H. Liang, E. Landais, X. Nie, L. K. Pritchard, M. Crispin, G. Kelsoe, I.A. Wilson, H. Schuitemaker, P.J. Klasse, J. P. Moore, D.R. Burton, A.B. Ward, R.W. Sanders, An HIV-1 antibody from an elite neutralizer implicates the fusion peptide as a site of vulnerability, Nat. Microbiol. 2 (2017). Art. No. 16199.
[14] K. Xu, P. Acharya, R. Kong, C. Cheng, G.-Y. Chuang, K. Liu, M.K. Louder, S. O'Dell, R. Rawi, M. Sastry, C.-H. Shen, B. Zhang, T. Zhou, M. Asokan, R.T. Bailer, M. Chambers, X. Chen, C.W. Choi, V.P. Dandey, N.A. Doria-Rose, A. Druz, E.T. Eng, S.K. Farney, K.E. Foulds, H. Geng, I.S. Georgiev, J. Gorman, K.R. Hill, A.J. Jafari, Y. D. Kwon, Y.-T. Lai, T. Lemmin, K. McKee, T.Y. Ohr, L. Ou, D. Peng, A.P. Rowshan, Z. Sheng, J.-P. Todd, Y. Tsybovsky, E.G. Viox, Y. Wang, H. Wei, Y. Yang, A.F. Zhou, R. Chen, L. Yang, D.G. Scorpio, A.B. McDermott, L. Shapiro, B. Carragher, C. S. Potter, J.R. Mascola, P.D. Kwong, Epitope-based vaccine design yields fusion peptide-directed antibodies that neutralize diverse strains of HIV-1, Nat. Med. 24 (2018) 857–867.
[15] C.P. Jaroniec, J.D. Kaufman, S.J. Stahl, M. Viard, R. Blumenthal, P.T. Wingfield, A. Bax, Structure and dynamics of micelle-associated human immunodeficiency virus gp41 fusion domain, Biochemistry 44 (2005) 16167–16180.
[16] C.M. Gabrys, D.P. Weliky, Chemical shift assignment and structural plasticity of a HIV fusion peptide derivative in dodecylphosphocholine micelles, Biochim. Biophys. Acta 1768 (2007) 3225–3234.
[17] Y.L. Li, L.K. Tamm, Structure and plasticity of the human immunodeficiency virus gp41 fusion domain in lipid micelles and bilayers, Biophys. J. 93 (2007) 876–885.
[18] W. Qiang, M.L. Bodner, D.P. Weliky, Solid-state NMR spectroscopy of human immunodeficiency virus fusion peptides associated with host-cell-like membranes: 2D correlation spectra and distance measurements support a fully extended conformation and models for specific antiparallel strand registries, J. Am. Chem. Soc. 130 (2008) 5459–5471.
[19] S.D. Schmick, D.P. Weliky, Major antiparallel and minor parallel beta sheet populations detected in the membrane-associated Human Immunodeficiency Virus fusion peptide, Biochemistry 49 (2010) 10623–10635.
[20] S.D. Schmick, High Resolution Tertiary Structure of the Membrane-Asssociated HIV Fusion Peptides by Solid State Nuclear Magnetic Resonance, Michigan State University, East Lansing, MI, USA, 2012.
[21] K. Sackett, M.J. Nethercott, Z.X. Zheng, D.P. Weliky, Solid-state NMR spectroscopy of the HIV gp41 membrane fusion protein supports intermolecular antiparallel beta sheet fusion peptide structure in the final six-helix bundle state, J. Mol. Biol. 426 (2014) 1077–1094.
[22] N.A. Lakomek, J.D. Kaufman, S.J. Stahl, J.M. Louis, A. Grishaev, P.T. Wingfield, A. Bax, Internal dynamics of the homotrimeric HIV-1 viral coat protein gp41 on multiple time scales, Angew. Chem. Int. Ed. 52 (2013) 3911–3915.
[23] P.U. Ratnayake, K. Sackett, M.J. Nethercott, D.P. Weliky, pH-dependent vesicle fusion induced by the ectodomain of the human immunodeficiency virus membrane fusion protein gp41: Two kinetically distinct processes and fully-membrane-associated gp41 with predominant beta sheet fusion peptide conformation, Biochim. Biophys. Acta 1848 (2015) 289–298.
[24] K. Sackett, M.J. Nethercott, Y. Shai, D.P. Weliky, Hairpin folding of HIV gp41 abrogates lipid mixing function at physiologic pH and inhibits lipid mixing by exposed gp41 constructs, Biochemistry 48 (2009) 2714–2722.
[25] S. Liang, P.U. Ratnayake, C. Keinath, L. Jia, R. Wolfe, A. Ranaweera, D.P. Weliky, Efficient fusion at neutral pH by Human Immunodeficiency Virus gp41 trimers containing the fusion peptide and transmembrane domains, Biochemistry 57 (2018) 1219–1235.
[26] T. Suarez, W.R. Gallaher, A. Agirre, F.M. Goni, J.L. Nieva, Membrane interface-interacting sequences within the ectodomain of the human immunodeficiency virus type 1 envelope glycoprotein: putative role during viral fusion, J. Virol. 74 (2000) 8038–8047.
[27] M. Montero, N.E. van Houten, X. Wang, J.K. Seott, The membrane-proximal external region of the human immunodeficiency virus type 1 envelope: dominant site of antibody neutralization and target for vaccine design, Microbiol. Mol. Biol. Rev. 72 (2008) 54–84.
[28] Z.Y.J. Sun, K.J. Oh, M.Y. Kim, J. Yu, V. Brusic, L.K. Song, Z.S. Qiao, J.H. Wang, G. Wagner, E.L. Reinherz, HIV-1 broadly neutralizing antibody extracts its epitope from a kinked gp41 ectodomain region on the viral membrane, Immunity 28 (2008) 52–63.
[29] B. Apellaniz, E. Rujas, S. Serrano, K. Morante, K. Tsumoto, J.M.M. Caaveiro, M. Angeles Jimenez, J.L. Nieva, The atomic structure of the HIV-1 gp41 transmembrane domain and its connection to the immunogenic membrane-proximal external region, J. Biol. Chem. 290 (2015) 12999–13015.
[30] S.C. Chiliveri, J.M. Louis, R. Ghirlando, J.L. Baber, A. Bax, Tilted, uninterrupted, monomeric HIV-1 gp41 transmembrane helix from residual dipolar couplings, J. Am. Chem. Soc. 140 (2018) 34–37.
[31] Q.S. Fu, M.M. Shaik, Y.F. Cai, F. Ghantous, A. Piai, H.Q. Peng, S. Rits-Volloch, Z. J. Liu, S.C. Harrison, M.S. Seaman, B. Chen, J.J. Chou, Structure of the membrane proximal external region of HIV-1 envelope glycoprotein, Proc. Natl. Acad. Sci. U. S. A. 115 (2018). E8892–E8899.
[32] B. Kwon, M. Lee, A.J. Waring, M. Hong, Oligomeric structure and three-dimensional fold of the HIV gp41 membrane-proximal external region and transmembrane domain in phospholipid bilayers, J. Am. Chem. Soc. 140 (2018) 8246–8259.
[33] K. Banerjee, D.P. Weliky, Folded monomers and hexamers of the ectodomain of the HIV gp41 membrane fusion protein: Potential roles in fusion and synergy between the fusion peptide, hairpin, and membrane-proximal external region, Biochemistry 53 (2014) 7184–7198.
[34] M. Kielian, Mechanisms of virus membrane fusion proteins, Annu. Rev. Virol. 1 (2014) 171–189.
[35] S.C. Harrison, Viral membrane fusion, Virology 479 (2015) 498–507.

[36] S. Shnaper, K. Sackett, S.A. Gallo, R. Blumenthal, Y. Shai, The C- and the N-terminal regions of glycoprotein 41 ectodomain fuse membranes enriched and not enriched with cholesterol, respectively, J. Biol. Chem. 279 (2004) 18526–18534.
[37] J. Roche, J.M. Louis, A. Grishaev, J.F. Ying, A. Bax, Dissociation of the trimeric gp41 ectodomain at the lipid-water interface suggests an active role in HIV-1 Env-mediated membrane fusion, Proc. Natl. Acad. Sci. U. S. A. 111 (2014) 3425–3430.
[38] D.J. Benton, S.J. Gamblin, P.B. Rosenthal, J.J. Skehel, Structural transitions in influenza haemagglutinin at membrane fusion pH, Nature 583 (2020) 150–153.
[39] C. Aisenbrey, B. Bechinger, Structure, interactions and membrane topology of HIV gp41 ectodomain sequences, Biochim. Biophys. Acta 1862 (2020), 183274.
[40] M.W. Eller, H.M.H. Siaw, R.B. Dyer, Stability of HA2 prefusion structure and pH-induced conformational changes in the HA2 domain of H3N2 hemagglutinin, Biochemistry 60 (2021) 2623–2636.
[41] M. Lee, C.A. Morgan, M. Hong, Fully hydrophobic HIV gp41 adopts a hemifusion-like conformation in phospholipid bilayers, J. Biol. Chem. 294 (2019) 14732–14744.
[42] E. Leikina, D.L. LeDuc, J.C. Macosko, R. Epand, Y.K. Shin, L.V. Chernomordik, The 1-127 HA2 construct of influenza virus hemagglutinin induces cell-cell hemifusion, Biochemistry 40 (2001) 8378–8386.
[43] N. Lev, Y. Fridmann-Sirkis, L. Blank, A. Bitler, R.F. Epand, R.M. Epand, Y. Shai, Conformational stability and membrane interaction of the full-length ectodomain of HIV-1 gp41: Implication for mode of action, Biochemistry 48 (2009) 3166–3175.
[44] K. Sackett, M.J. Nethercott, R.F. Epand, R.M. Epand, D.R. Kindra, Y. Shai, D. P. Weliky, Comparative analysis of membrane-associated fusion peptide secondary structure and lipid mixing function of HIV gp41 constructs that model the early pre-hairpin intermediate and final hairpin conformations, J. Mol. Biol. 397 (2010) 301–315.
[45] K. Sackett, A. TerBush, D.P. Weliky, HIV gp41 six-helix bundle constructs induce rapid vesicle fusion at pH 3.5 and little fusion at pH 7.0: understanding pH dependence of protein aggregation, membrane binding, and electrostatics, and implications for HIV-host cell fusion, Eur. Biophys. J. 40 (2011) 489–502.
[46] C.S. Kim, R.F. Epand, E. Leikina, R.M. Epand, L.V. Chernomordik, The final conformation of the complete ectodomain of the HA2 subunit of Influenza Hemagglutinin can by itself drive low pH-dependent fusion, J. Biol. Chem. 286 (2011) 13226–13234.
[47] A. Pabis, R.J. Rawle, P.M. Kasson, Influenza hemagglutinin drives viral entry via two sequential intramembrane mechanisms, Proc. Natl. Acad. Sci. U. S. A. 117 (2020) 7200–7207.
[48] P. Larsson, P.M. Kasson, Lipid tail protrusion in simulations predicts fusogenic activity of influenza fusion peptide mutants and conformational models, PLoS Comp. Biol. 9 (2013) e1002950.
[49] U. Ghosh, D.P. Weliky, ^{2}H nuclear magnetic resonance spectroscopy supports larger amplitude fast motion and interference with lipid chain ordering for membrane that contains beta sheet human immunodeficiency virus gp41 fusion peptide or helical hairpin influenza virus hemagglutinin fusion peptide at fusogenic pH, Biochim. Biophys. Acta 1862 (2020), 183404.
[50] U. Ghosh, D.P. Weliky, Rapid ^{2}H NMR transverse relaxation of perdeuterated lipid acyl chains of membrane with bound viral fusion peptide supports large-amplitude motions of these chains that can catalyze membrane fusion, Biochemistry 60 (2021) 2637–2651.
[51] A.L. Lai, J.H. Freed, HIV gp41 fusion peptide increases membrane ordering in a cholesterol-dependent fashion, Biophys. J. 106 (2014) 172–181.
[52] S.T. Smrt, A.W. Draney, J.L. Lorieau, The influenza hemagglutinin fusion domain is an amphipathic helical hairpin that functions by inducing membrane curvature, J. Biol. Chem. 290 (2015) 228–238.
[53] G. Meher, H. Chakraborty, The role of fusion peptides in depth-dependent membrane organization and dynamics in promoting membrane fusion, Chem. Phys. Lipids 234 (2021), 105025.
[54] E.O. Freed, E.L. Delwart, G.L. Buchschacher Jr., A.T. Panganiban, A mutation in the human immunodeficiency virus type 1 transmembrane glycoprotein gp41 dominantly interferes with fusion and infectivity, Proc. Natl. Acad. Sci. U. S. A. 89 (1992) 70–74.
[55] O.F. Brandenberg, C. Magnus, R.R. Regoes, A. Trkola, The HIV-1 entry process: a stoichiometric view, Trends Microbiol. 23 (2015) 763–774.
[56] P. Zhu, J. Liu, J. Bess, E. Chertova, J.D. Lifson, H. Grise, G.A. Ofek, K.A. Taylor, K. H. Roux, Distribution and three-dimensional structure of AIDS virus envelope spikes, Nature 441 (2006) 847–852.
[57] R. Sougrat, A. Bartesaghi, J.D. Lifson, A.E. Bennett, J.W. Bess, D.J. Zabransky, S. Subramaniam, Electron tomography of the contact between T cells and SIV/HIV-1: implications for viral entry, PLoS Pathog. 3 (2007) e63.
[58] F.B. Pereira, F.M. Goni, J.L. Nieva, Liposome destabilization induced by the HIV-1 fusion peptide effect of a single amino acid substitution, FEBS Lett. 362 (1995) 243–246.
[59] Y. Kliger, A. Aharoni, D. Rapaport, P. Jones, R. Blumenthal, Y. Shai, Fusion peptides derived from the HIV type 1 glycoprotein 41 associate within phospholipid membranes and inhibit cell-cell fusion. Structure-function study, J. Biol. Chem. 272 (1997) 13496–13505.
[60] C.M. Gabrys, W. Qiang, Y. Sun, L. Xie, S.D. Schmick, D.P. Weliky, Solid-state nuclear magnetic resonance measurements of HIV fusion peptide ^{13}CO to lipid ^{31}P proximities support similar partially inserted membrane locations of the α Helical and β sheet peptide structures, J. Phys. Chem. A 117 (2013) 9848–9859.
[61] F.B. Pereira, F.M. Goni, A. Muga, J.L. Nieva, Permeabilization and fusion of uncharged lipid vesicles induced by the HIV-1 fusion peptide adopting an extended conformation: dose and sequence effects, Biophys. J. 73 (1997) 1977–1986.
[62] P.W. Mobley, A.J. Waring, M.A. Sherman, L.M. Gordon, Membrane interactions of the synthetic N-terminal peptide of HIV-1 gp41 and its structural analogs, Biochim. Biophys. Acta 1418 (1999) 1–18.
[63] S. Kamath, T.C. Wong, Membrane structure of the human immunodeficiency virus gp41 fusion domain by molecular dynamics simulation, Biophys. J. 83 (2002) 135–143.
[64] W. Qiang, Y. Sun, D.P. Weliky, A strong correlation between fusogenicity and membrane insertion depth of the HIV fusion peptide, Proc. Natl. Acad. Sci. U. S. A. 106 (2009) 15314–15319.
[65] A. Jacobs, C. Simon, M. Caffrey, Thermostability of the HIV gp41 wild-type and loop mutations, *Protein Pept.* Lett. 13 (2006) 477–480.
[66] R. Yang, M. Prorok, F.J. Castellino, D.P. Weliky, A trimeric HIV-1 fusion peptide construct which does not self-associate in aqueous solution and which has 15-fold higher membrane fusion rate, J. Am. Chem. Soc. 126 (2004) 14722–14723.
[67] A.L. Lai, A.E. Moorthy, Y.L. Li, L.K. Tamm, Fusion activity of HIV gp41 fusion domain is related to its secondary structure and depth of membrane insertion in a cholesterol-dependent fashion, J. Mol. Biol. 418 (2012) 3–15.
[68] M. Lorizate, T. Sachsenheimer, B. Glass, A. Habermann, M.J. Gerl, H.G. Krausslich, B. Brugger, Comparative lipidomics analysis of HIV-1 particles and their producer cell membrane in different cell lines, Cell. Microbiol. 15 (2013) 292–304.
[69] J.C. Macosko, C.H. Kim, Y.K. Shin, The membrane topology of the fusion peptide region of influenza hemagglutinin determined by spin-labeling EPR, J. Mol. Biol. 267 (1997) 1139–1148.
[70] E. Zaitseva, E. Zaitsev, K. Melikov, A. Arakelyan, M. Marin, R. Villasmil, L. B. Margolis, G.B. Melikyan, L.V. Chernomordik, Fusion stage of HIV-1 entry depends on virus-induced cell surface exposure of phosphatidylserine, Cell Host Microbe 22 (2017) 99–110.
[71] R.F.M. de Almeida, L.M.S. Loura, A. Fedorov, M. Prieto, Lipid rafts have different sizes depending on membrane composition: a time-resolved fluorescence resonance energy transfer study, J. Mol. Biol. 346 (2005) 1109–1120.
[72] Y.H. Chen, J.T. Yang, K.H. Chau, Determination of helix and beta-form of proteins in aqueous-solution by circular-dichroism, Biochemistry 13 (1974) 3350–3359.
[73] G.F. Gao, L. Wieczorek, K.K. Peachman, V.R. Polonis, C.R. Alving, M. Rao, V. B. Rao, Designing a soluble near full-length HIV-1 gp41 trimer, J. Biol. Chem. 288 (2013) 234–246.
[74] M. Caffrey, J. Kaufman, S. Stahl, P. Wingfield, A.M. Gronenborn, G.M. Clore, Monomer-trimer equilibrium of the ectodomain of SIV gp41: insight into the mechanism of peptide inhibition of HIV infection, Protein Sci. 8 (1999) 1904–1907.
[75] A. Rath, M. Glibowicka, V.G. Nadeau, G. Chen, C.M. Deber, Detergent binding explains anomalous SDS-PAGE migration of membrane proteins, Proc. Natl. Acad. Sci. U. S. A. 106 (2009) 1760–1765.
[76] W. Shu, H. Ji, M. Lu, Interactions between HIV-1 gp41 core and detergents and their implications for membrane fusion, J. Biol. Chem. 275 (2000) 1839–1845.
[77] J. Chen, J.J. Skehel, D.C. Wiley, N- and C-terminal residues combine in the fusion-pH influenza hemagglutinin HA_2 subunit to form an N cap that terminates the triple-stranded coiled coil, Proc. Natl. Acad. Sci. U. S. A. 96 (1999) 8967–8972.
[78] A. Ranaweera, P.U. Ratnayake, E.A.P. Ekanayaka, R. Declercq, D.P. Weliky, Hydrogen-deuterium exchange supports independent membrane-interfacial fusion peptide and transmembrane domains in subunit 2 of influenza virus hemagglutinin protein, a structured and aqueous-protected connection between the fusion peptide and soluble ectodomain, and the importance of membrane apposition by the trimer-of-hairpins structure, Biochemistry 58 (2019) 2432–2446.
[79] J.L. Lorieau, J.M. Louis, A. Bax, The complete influenza hemagglutinin fusion domain adopts a tight helical hairpin arrangement at the lipid: water interface, Proc. Natl. Acad. Sci. U. S. A. 107 (2010) 11341–11346.
[80] U. Ghosh, L. Xie, L.H. Jia, S. Liang, D.P. Weliky, Closed and semiclosed interhelical structures in membrane vs closed and open structures in detergent for the Influenza Virus hemagglutinin fusion peptide and correlation of hydrophobic surface area with fusion catalysis, J. Am. Chem. Soc. 137 (2015) 7548–7551.
[81] A. Ranaweera, P.U. Ratnayake, D.P. Weliky, The stabilities of the soluble ectodomain and fusion peptide hairpins of the Influenza virus hemagglutinin subunit II protein are positively correlated with membrane fusion, Biochemistry 57 (2018) 5480–5493.
[82] H. Qiao, R.T. Armstrong, G.B. Melikyan, F.S. Cohen, J.M. White, A specific point mutant at position 1 of the influenza hemagglutinin fusion peptide displays a hemifusion phenotype, Mol. Biol. Cell 10 (1999) 2759–2769.
[83] E. Borrego-Diaz, M.E. Peeples, R.M. Markosyan, G.B. Melikyan, F.S. Cohen, Completion of trimeric hairpin formation of influenza virus hemagglutinin promotes fusion pore opening and enlargement, Virology 316 (2003) 234–244.
[84] Z. Dai, Y.S. Tao, N.N. Liu, M.D. Brenowitz, M.E. Girvin, J.R. Lai, Conditional trimerization and lytic activity of HIV-1 gp41 variants containing the membrane-associated segments, Biochemistry 54 (2015) 1589–1599.
[85] C. Grewe, A. Beck, H.R. Gelderblom, HIV: early virus-cell interactions, J. AIDS 3 (1990) 965–974.
[86] N. Herold, M. Anders-Osswein, B. Glass, M. Eckhardt, B. Muller, H.G. Krausslich, HIV-1 entry in SupT1-R5, CEM-ss, and primary CD4(+) T Cells occurs at the plasma membrane and does not require endocytosis, J. Virol. 88 (2014) 13956–13970.
[87] G.B. Melikyan, HIV entry: a game of hide-and-fuse? Curr. Opin. Virol. 4 (2014) 1–7.

Supplementary Material for "*A large HIV gp41 construct with trimer-of-hairpins structure exhibits V2E mutation-dominant attenuation of vesicle fusion and helicity very similar to V2E attenuation of HIV fusion and infection and supports: (1) hairpin stabilization of membrane apposition with larger distance for V2E; and (2) V2E dominance by an antiparallel β sheet with interleaved fusion peptide strands from two gp41 trimers*"

Md. Rokonujjaman, Abdulrazak Sahyouni, Robert Wolfe, Lihui Jia, Ujjayini Ghosh, and David P. Weliky

Department of Chemistry, Michigan State University, East Lansing, MI, 48824, USA

Figure S1. DNA sequence of Wild-type FP_HM including non-native G_6LEH_6 C-terminal tag. For the V2E mutant, the T nucleotide at the fifth position is replaced by A.

```
1   GCCGTGGGTATCGGTGCTCTGTTCCTGGGTTTCCTGGGTGCTGCTGGTTCGACGATGGGTGCCCGCTCAATGACG
76  CTGACGGTCCAAGCACGTCAGCTGCTGAGCGGCATTGTGCAGCAACAGAACAATCTGCTGCGCGCGATCGAAGCC
151 CAACAGCATCTGCTGCAGCTGACCGTTTGGGGTATTAAACAACTGCAGGCTCGTATCCTGAGCGGCGGTCGCGGC
226 GGTTGGATGGAATGGGATCGTGAAATTAACAATTATACGAGCCTGATTCACTCTCTGATCGAAGAAAGTCAAAAC
301 CAACAGGAGAAAAACGAACAGGAACTGCTGGAACTGGACAAATGGGCCTCCCTGTGGAACTGGTTTAACATTACG
376 AACTGGCTGTGGTACATCAAAGGCGGCGGTGGCGGTGGTCTCGANCACCACCACCACCACCAC
```

Figure S2. Primer nucleotide sequences to produce V2E_FPHM mutant

Forward Primer Sequence: 5′- CAT ATG GCC GAG GGT ATC GGT G- 3′

Reverse Primer Sequence: 5′- CAC CGA TAC CCT CGG CCA TAT G- 3′

Figure S3. Protein sequence coverage from mass spectrometry of peptides formed from trypsin digestion. The highlighted yellow residues were in a peptide. The highlighted green residues were in peptides but had mass changes consistent with oxidation (M), deamination (Q), or dehydration (E).

Wild-type

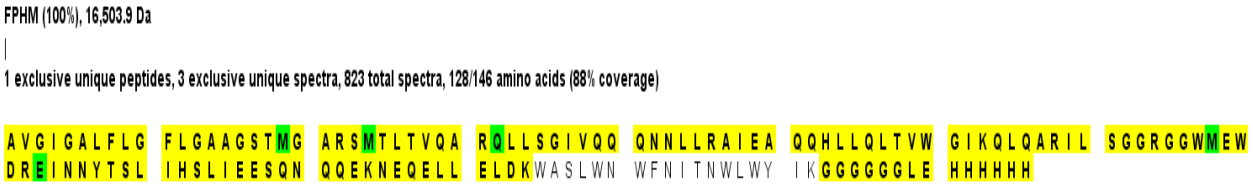

V2E

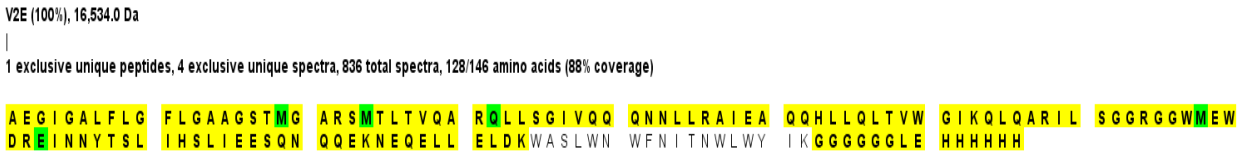

Figure S4. CD spectra of (A) Wild-type and (B) V2E mutant FP_HM at temperatures between 22 and 95 °C. All spectra were recorded on the same day with [protein] ≈ 6 μM in 10 mM Tris buffer at pH 7.4 with 0.2% SDS. The WT and V2E FP_HM are from different preparations than those used for the CD spectra in Fig. 3A,B in the main text. The spectra are consistent with helical structure based on shallow minima near 208 and 222 nm. At 22 °C, the $|\theta_{222}|$ values for WT and V2E are 1.82×10^4 and 1.54×10^4 deg-cm^2-dmol^{-1}, respectively, which correspond to 55% and 47% helicity. The CD spectra in Fig. 3A,B in the main text similarly show 9% greater helicity for WT vs. V2E mutant FP_HM.

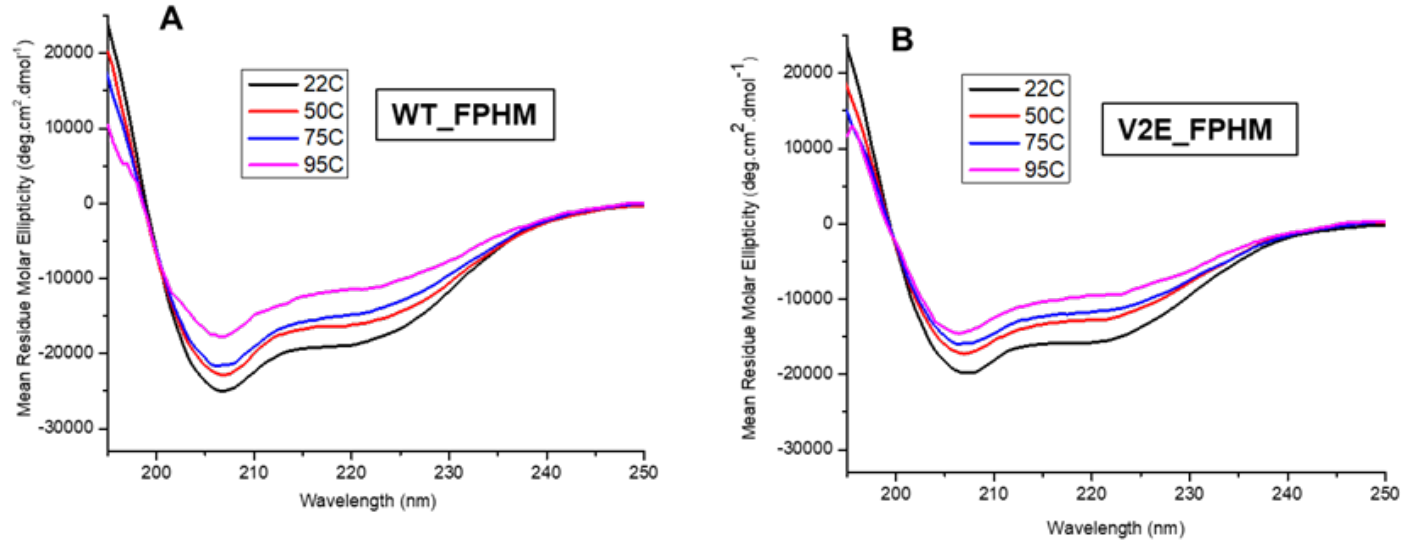

Figure S5. Size-exclusion chromatography of molecular weight standards using A_{280} detection.

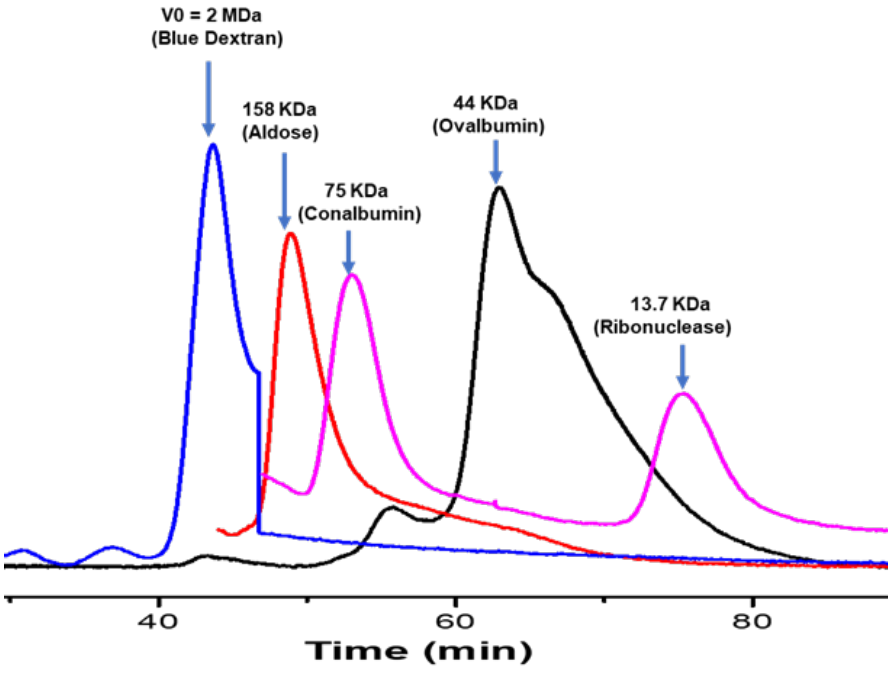

Figure S6. Vesicle fusion assays at 37 ºC and FP_HM:lipid molar ratios of (A) 1:100 and (B) 1:300. The 1:100 data are a second trial and were obtained with a different batch of vesicles and different FP_HM stocks than Fig. 6 in the main text. At time = 0, an aliquot of FP_HM stock was added to the vesicle solution. The vesicle solution had [total lipid] = 150 μM at pH 5.3 with POPC:POPG (4:1) composition. The FP_HM stock had 150 μM FP_HM in 10 mM Tris buffer at pH 7.4 with 0.2% SDS.

A FP_HM:lipid = 1:100 (second trial)

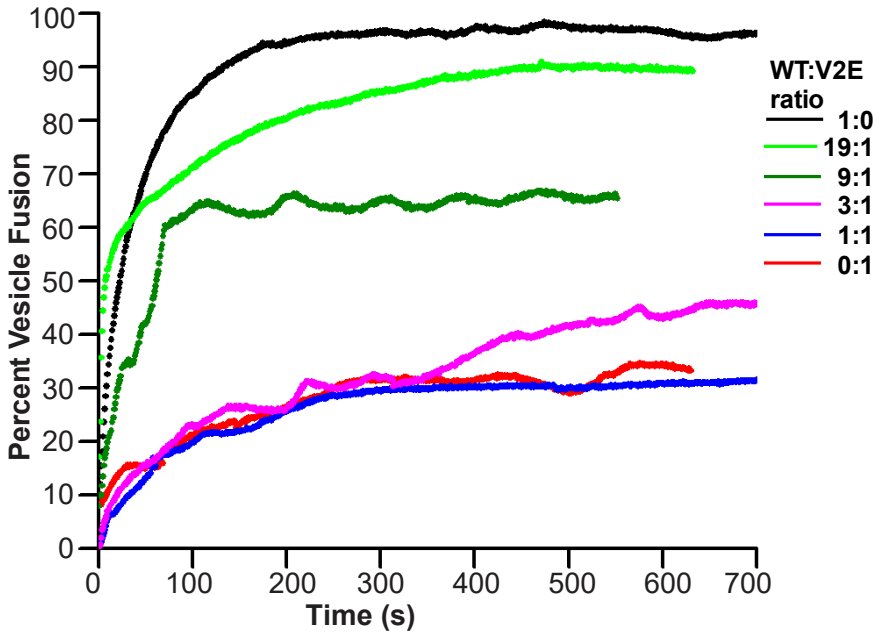

B FP_HM:lipid = 1:300